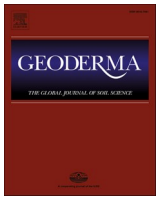
Geoderma 475 (2026) 118084



Contents lists available at ScienceDirect

Geoderma

journal homepage: www.elsevier.com/locate/geoderma



Behavior of lithium during soil formation: lithium signatures in soil minerals derived from Li–pegmatites

P. Louis Lu [a,*], Russell S. Harmon [b], Lamont Leatherman [c], Gordon D.Z. Williams [a], Adam C. Curry [d], Leon Kelly [a], Gary S. Dwyer [a], Valerie S. Reynolds [e], S. Anselme Dossou [a], Daniel D. Richter [a]

[a] Division of Earth and Climate Sciences, Nicholas School of the Environment, Duke University, NC, 27708, USA
[b] Department of Marine, Earth and Atmospheric Sciences, North Carolina State University, Raleigh, NC, 27607, USA
[c] Formerly at Piedmont Lithium Inc., 42 E Catawba Street, Belmont, NC, 28012, USA
[d] Department of Earth, Marine, and Environmental Sciences, University of North Carolina, Chapel Hill, NC, 27599, USA
[e] Department of Earth, Environmental, and Geographical Sciences, University of North Carolina at Charlotte, Charlotte, NC, 28223, USA

ARTICLE INFO

Handling Editor: Dr Alberto Agnelli

Keywords:
Soil lithium
Weathering and pedogenesis
Li-pegmatite exploration
Soil prospecting
Critical minerals
Li isotopes
US southern piedmont
Carolina tin-spodumene belt

ABSTRACT

Lithium (Li) is a critical metal for technology development which is driving demand and increasing exploration for new resources. Granite pegmatites represent an important natural source of Li. Soil analysis during geological exploration can provide important insights into the presence of buried pegmatites. Here, we assert that understanding soil and regolith formation and the behavior of Li and associated pathfinder elements can enhance mineral prospecting. This study applies a pedological approach to investigate the physiochemical, mineralogical, and isotopic properties of soil-weathering profiles produced by spodumene-bearing pegmatites and surrounding country rock in the Carolina Tin-Spodumene Belt in south-central North Carolina, USA. Markedly higher Li concentrations are present in soils directly above Li-pegmatite dikes compared to off-dike soils, with > 80 % of the original Li lost during weathering across the above-dike soil profiles. Relic primary Li–rich minerals, spodumene and muscovite, are the main mineral phases responsible for soil Li signatures overlying the dikes. Exchangeable Li represents a negligible fraction of total Li in both above- and off-dike soils. Secondary mineral phases such as Fe, Al, and Mn oxyhydroxides appear to scavenge similar amounts of Li but account for a larger fraction of the total Li pool in off-dike soils. Li-isotope signatures (δ^7Li) are systematically depleted in off-dike soils, clay fractions, and oxide-associated fractions. Variability of Li within soil-weathering profiles reflects surface mixing, heterogeneity of bedrock lithology, and textural differences caused by eluviation and illuviation. Integrating pedological and geochemical perspectives can, therefore, enhance the value of soil geochemical surveys for Li-pegmatite exploration.

1. Introduction

Lithium (Li) has emerged as an important critical metal for technology development, particularly for Li-ion batteries which support new energy technologies such as electric vehicles and grid-scale energy storage. Accelerated demand for Li highlights the need for advanced exploration techniques and optimized production pathways (IEA, 2021, Reich and Simon, 2025).

Granite pegmatites are a vital resource of Li (Bradley and McCauley, 2013, Bradley et al., 2017; Benson et al., 2025). Li-rich pegmatites belong to Group 1 pegmatites in the classification system of Wise et al. (2022a) and broadly correspond to the Lithium-Cesium-Tantalum (LCT) pegmatite type of Černý and Ercit (2005). Hereafter, these pegmatites are referred to interchangeably as “Group 1 pegmatites,” “Li-pegmatites,” or “spodumene-bearing pegmatites.”

Soil and regolith analysis is an emerging approach that has been applied to Li-pegmatite exploration (e.g. Harmon et al., 2025). Being commonly regarded as ‘overburden’ in an exploration context, soils may carry, obscure, or homogenize elemental signals from the underlying rocks, thereby introducing uncertainty into exploration programs (Anand et al., 2007; Noble et al., 2013). However, careful application of soil geochemistry can reduce environmental disturbance relative to

* Corresponding author at: Nicholas School of the Environment, Duke University, 9 Circuit Dr, Durham, NC 27708, USA.
E-mail address: louis.lu@duke.edu (P.L. Lu).

https://doi.org/10.1016/j.geoderma.2026.118084
Received 13 February 2026; Received in revised form 8 October 2026; Accepted 9 October 2026
Available online 30 October 2026
0016-7061/© 2026 The Authors. Published by Elsevier B.V. This is an open access article under the CC BY license (http://creativecommons.org/licenses/by/4.0/).

trenching and coring, enhance exploration efficiency (Noble et al., 2020; Demetriades et al., 2018), and even detect concealed ore bodies (e.g., Xu et al., 2019).

Previous studies have developed a diverse suite of soil Li pathfinders (i.e. geochemical tracers), including total Li concentration, elemental ratios (e.g. K/Rb, Rb/Sr), and isotopic signatures (e.g. $^{87}Sr/^{86}Sr$), and employed the use of machine-learning approaches based on multiple parameters to improve predictions for the presence of underlying Li-pegmatite ore bodies. Some of these techniques have been combined with rapid-analysis techniques such as handheld LIBS and portable XRF to enhance in-field exploration (Hall et al., 2025; Harmon et al., 2025; Harmon et al., 2023; Pierangeli et al., 2025; Wise et al., 2022b). While soil sampling and analysis may be included in geological exploration, such soil characterization often focuses on surficial horizons or a single depth and is typically restricted to analyzing bulk elemental concentrations (e.g. Harmon et al., 2025; Pierangeli et al., 2025). These approaches are practical and align well with exploration objectives but leave the processes of weathering and pedogenesis unaddressed that control soil geochemistry and the fate of Li in pegmatite-derived soil systems (Sirbescu et al., 2025).

Despite recent advances in pegmatite geochemistry and soil-based Li exploration, studies have yet to characterize soils in Group 1 pegmatite systems in a pedological framework. In particular, soil-forming processes that govern the distribution, mobility, and preservation of Li and associated pathfinder elements within residual soil profiles are not well understood.

Soils develop through the physical, chemical, and biological weathering of bedrock and sediments. As erosion lowers the land surface, the underlying rock is progressively exhumed and broken down into smaller particles that are conveyed into the overlying regolith layer, a process often described as soil production (Dietrich et al., 1995), mobile regolith production (Anderson et al., 2013), and the soil–particle conveyor (Richter et al., 2020). Through this process, signatures of metals and trace elements such as Li can be substantially modified by chemical weathering, secondary mineral formation, and soil horizonation (Huh et al., 2004; Steinhoefel et al., 2021; Brantley and Lebedeva, 2011). Biological factors, including vegetation, soil fauna, and microorganisms, also play important roles in soil formation by influencing mineral weathering, element cycling, and pedoturbation (Paton et al., 1995). Such effects have critical implications for exploration targeting, the depth and extent of sampling, and interpretation of anomalies. This can be particularly important to the relatively well-developed, clay-rich soils found in warm, moisture-sufficient tropical and temperate climates, where enhanced weathering commonly produces thick soil mantles. These soils represent about half (44 %) of those overlying Group 1 pegmatite deposits worldwide (Fig. 1; Table S1; Benson et al., 2025) and are commonly subject to pedogenic processes such as eluviation, illuviation, and leaching that are characteristic of moderate to advanced weathering (Buol et al., 2011), making them ideal natural systems for examining how pedogenesis shapes the redistribution of trace elements such as Li in soils.

Lithium is a highly soluble alkali metal and is readily released from primary minerals during weathering. Therefore, the Li content of soils is largely governed by conditions of their formation rather than by Li concentration in bedrock. As a consequence, the distribution of Li in soil-weathering profiles can be highly irregular (Kabata-Pendias, 2011). Previous studies have demonstrated the high mobility of Li during pedogenesis (Luecke, 1984; Middelburg et al., 1988; Singh and Gilkes, 1993). For example, Singh and Gilkes (1993) observed a near total loss of Li during the transformation of spodumene [$LiAlSi_2O_6$] to secondary smectites in a lateritic environment in Western Australia. Analyzing soils above a Li-pegmatite dike in southeast Ireland, Luecke (1984) undertook one of the first depth-resolved soil Li geochemistry studies and observed enrichment of Li and other trace metals in the illuviated subsoil horizons and relatively lower concentrations in surficial and saprolitic horizons. Both studies illustrated how pedogenesis influenced soil Li distribution and underscored the need to understand the mechanisms controlling the fate of Li in soils in order to explain its depth-distribution patterns.

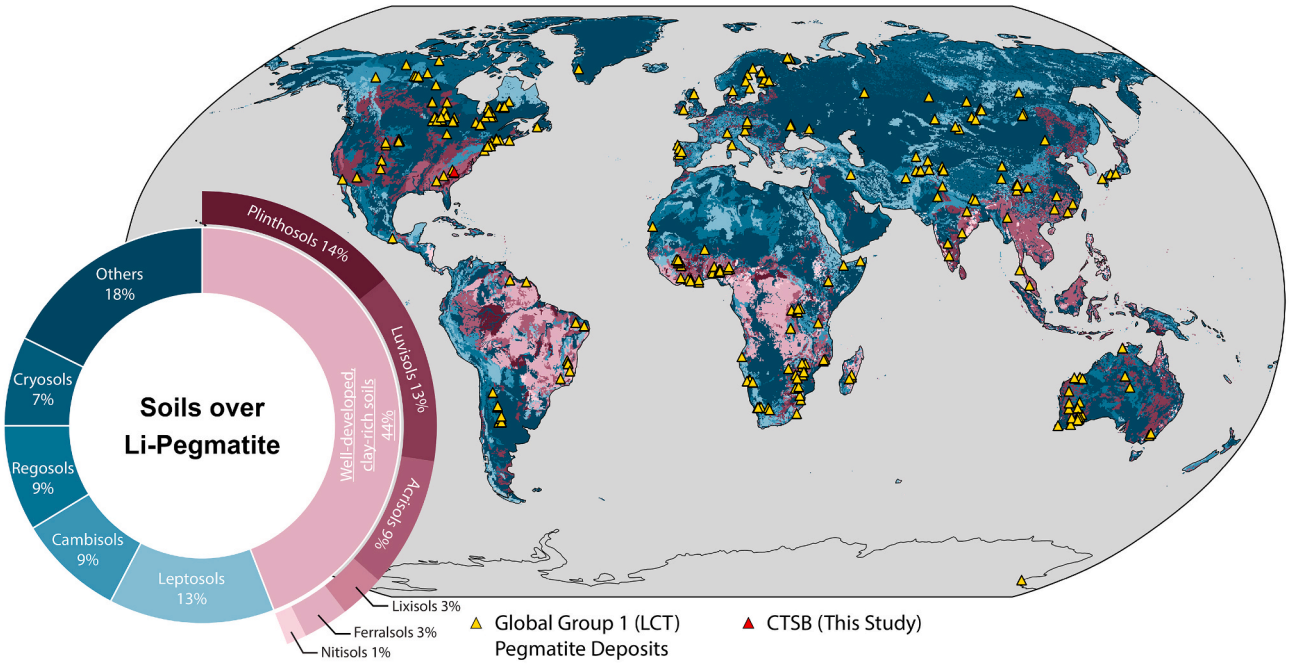


Fig. 1. Global distribution of Group 1 (or LCT) pegmatite deposits and their associated dominant soil groups classified using the World Reference Base (WRB) system, with the Carolina Tin-Spodumene Belt (CTSB; where the present study was conducted) highlighted. The donut chart serves as the legend for the mapped soil groups and summarizes their relative proportions at pegmatite deposit locations. Well-developed, clay-rich soils (including Acrisols, Ferralsols, Luvisols, Lixisols, Nitisols, and Plinthosols) constitute the largest fraction (~44 %), followed by Leptosols (~13 %), Cambisols (~9 %), Regosols (~9 %), Cryosols (~7 %), and others (~18 %). Among these, Acrisols and many Nitisols correspond broadly to the USDA Soil Taxonomy order Ultisols, which characterizes the soils studied at our field site. Data compiled from Benson et al. (2025) and the Harmonized World Soil Database (HWSD) v 2.0 (FAO, and IIASA., 2023).

The retention of Li by soils is commonly attributed to its sequestration by secondary clay and oxide minerals (Ashry 1973; Starkey, 1982; Kim and Grey, 2010; Hoyer et al., 2015). Positive associations between soil Li content and both the type and abundance of secondary clays have been reported in different soil systems. Anderson et al. (1988) observed such relationships in soils of the southeastern United States and estimated that water-soluble and exchangeable Li constituted a minor fraction (<1.1 %) of the total soil Li pool. Huh et al. (2004) demonstrated similar relationships across a weathering gradient in Hawaii but emphasized the role of the soil cation exchange capacity in influencing Li retention. Soil organic matter may also influence Li cycling and retention through plant uptake and litter decomposition (Robinson et al., 2018). Such mechanisms have regained significant attention following recent soil Li analysis conducted for mineral exploration (Hall et al., 2025; Harmon et al., 2025; Sirbescu et al., 2025), which highlight the need to clarify potential sinks of soil Li to account for its markedly elevated concentrations, i.e., with bulk soil containing up to 2500-ppm Li as reported by Harmon et al. (2025). In contrast to previous studies that focused on background levels of Li in soils not associated with mineralization, soils in granite pegmatite domains can be strongly enriched in Li. This raises the question of whether Li behaves the same way in such environments. Investigating soils formed over Florence County pegmatites in the glacial/periglacial landscapes in Wisconsin, Sirbescu et al. (2025) reported soil Li concentrations up to 1400 ppm and suggested that unweathered minerals serve as principal carriers of Li and associated pathfinders. However, their interpretation is based largely on field and qualitative observations rather than on direct quantitative characterization through size-fraction and chemical analyses. Also, the study area lies within a recently glaciated terrain with relatively young, thin soils. Whether soil Li retention follows similar patterns in older, more deeply weathered landscapes with thicker soil mantles remains to be investigated.

This study adopted a multi-faceted pedological approach to characterize Li-enriched soil and weathering profiles of the Carolina Tin-Spodumene Belt (CTSB), one of North America's largest pegmatite-Li districts hosting multiple historic mines. Situated in the subtropics of the warm and humid southeastern United States, the study area has well-developed, clay-rich Ultisols typical of much of the humid temperate and tropical zones worldwide, and provides a valuable context for investigating pedogenic controls on soil Li distributions and behavior. Through examining depth-dependent physical, chemical, mineralogical, and Li isotopic properties of soils formed directly above Li-pegmatite dikes and at nearby off-pegmatite-dike locations in the CTSB, we aim to identify the principal Li reservoirs contributing to soil Li signatures and to characterize the mechanisms governing the fate of Li during soil formation. We intend our findings to benefit future soil Li prospecting and provide a framework for investigating the pedogenic behavior of other trace and critical elements in soil and regolith systems.

2. Methods

2.1. Site description

The CTSB is a 3- to 5-km wide zone located within the southeastern Piedmont of the United States, where both common quartz-feldspar and spodumene-bearing Group 1 pegmatite (Wise et al., 2022a) intruded into Cambrian to Neoproterozoic country rock throughout the region during Carboniferous time (Kesler, 1942, 1976; Horton, 1981; Kish and Fullagar, 1996). Readers are referred to Swanson (2012) and Curry et al. (2025) for a comprehensive overview of the regional geology and geochemistry. Multiple episodes of pegmatite intrusion produced numerous dike-and-sill structures ranging from < 1 m to > 100 m in thickness that crosscut metamorphic country rocks, resulting in a landscape underlain by a heterogeneous ancient metamorphic and granitic bedrock that serves as the parent material for soil development.

Our research site is situated within a section of the CTSB located between Bessemer City and Lincolnton, North Carolina (Fig. 2A and B). Here, the combination of a generally warm and humid climate over much of the Quaternary, and prolonged landscape stability (conservatively > 2 Ma; Bacon et al., 2012) in the absence of continental glaciation has given rise to deeply weathered regolith and Ultisols that cover much of the Southern Piedmont. Although these Ultisols have long been interpreted as products of prolonged in–situ weathering of rock residuum, characterized by clay-rich and nutrient-poor subsoil Bt horizons typical of an advanced stage of weathering (Buol, 2003), recent work shows that many Piedmont soil profiles also record contributions from transported or reworked materials, reflecting their polygenetic nature (Richter et al., 2020). Bedrock in the sampling area is predominantly mapped as a mix of mica schist, amphibolite, and biotite gneiss (Horton et al., 2017), with soils derived from these lithologies mapped as Lloyd series (fine, kaolinitic, thermic Rhodic Kanhapludults) according to the USDA–NRCS SSURGO database (Soil Survey Staff, 2025) accessed via SoilWeb (Fig. 2A; O'Geen et al., 2017). The characteristic rhodic (dark red) color (2.5YR 3/6) of the Lloyd series reflects its derivation from relatively mafic to intermediate lithologies (amphibolite, schist, and gneiss) in contrast to the more felsic parent materials (granite and granitic gneiss) that produce the Cecil and Pacolet series soils (both fine, kaolinitic, thermic Typic Kanhapludults), with the latter distinguished by its thinner clayey horizons and occurrence in less stable landscape positions (Soil Survey Staff, 2025). Cecil and Pacolet soils are widespread across the Piedmont (Daniels et al., 1999) and are present in portions of our study area (Fig. 2A).

Three pairs of soil cores were collected above Li-pegmatite dikes and at off-dike positions over the surrounding country rock at three locations (sites A, B, and C) using a 10-cm-diameter bucket auger. Sites A and B were located along a known pegmatite dike situated approximately 5 to 15 m beneath the surface, whose presence and structure were determined from three independent exploratory drill core locations (Harmon et al., 2025) sited during an exploration program conducted by Piedmont Lithium Inc. Three above-dike cores were collected at these two sites, located ~100 m apart along the NE–SW-trending dike (one at Site A and two at Site B), along with one off-dike core at each site ~30 m laterally away upslope from the above-dike sampling locations (Fig. 2C). The upslope cores that overlie the country rock were chosen to represent off-dike profiles to avoid potential complications from hillslope sediments that could affect downslope locations.

Soil profiles were augered to a maximum depth of 2 m or until augering refusal, whichever came first, with the 2-meter depth defined operationally as the lower boundary for soil description and sampling. Samples were collected at 8 to 25 cm intervals from the surface to the bottom of each core, with the exact spacing adjusted based on augering resistance and changes in soil horizon characteristics.

A third set of soil profiles were sampled at Site C, approximately 1 km southeast of sites A and B, where previous drill cores indicated the presence of a Li-pegmatite dike at deeper depths greater than 20 m. Here, sampling was extended to 5 m to capture the deeper regolith and potential geochemical expression of the buried dike, with most samples obtained at 50 cm intervals as a practical sampling strategy for deeper and comparatively homogeneous profiles.

Each sample was carefully collected to avoid contamination from surficial soil within the auger hole, and the soil was thoroughly homogenized on a clean tarp before subsampling. Boulders and 'float' rocks of various sizes appeared sporadically on the soil surface above the pegmatite dike where sites A and B are located and along its projected surface trace (Fig. 2C), whereas no coarse surface fragments were present at Site C. Samples of spodumene pegmatite and amphibolite bedrock were collected from archived drill cores obtained during previous exploration drilling carried out by Piedmont Lithium.

As part of the southern Piedmont, the entire landscape has been shaped by some two centuries of cultivation and pasture agriculture (Daniels, 1987, Richter et al., 2020). Based on historical aerial photographs and their interpretation, sites A and B were old agricultural fields

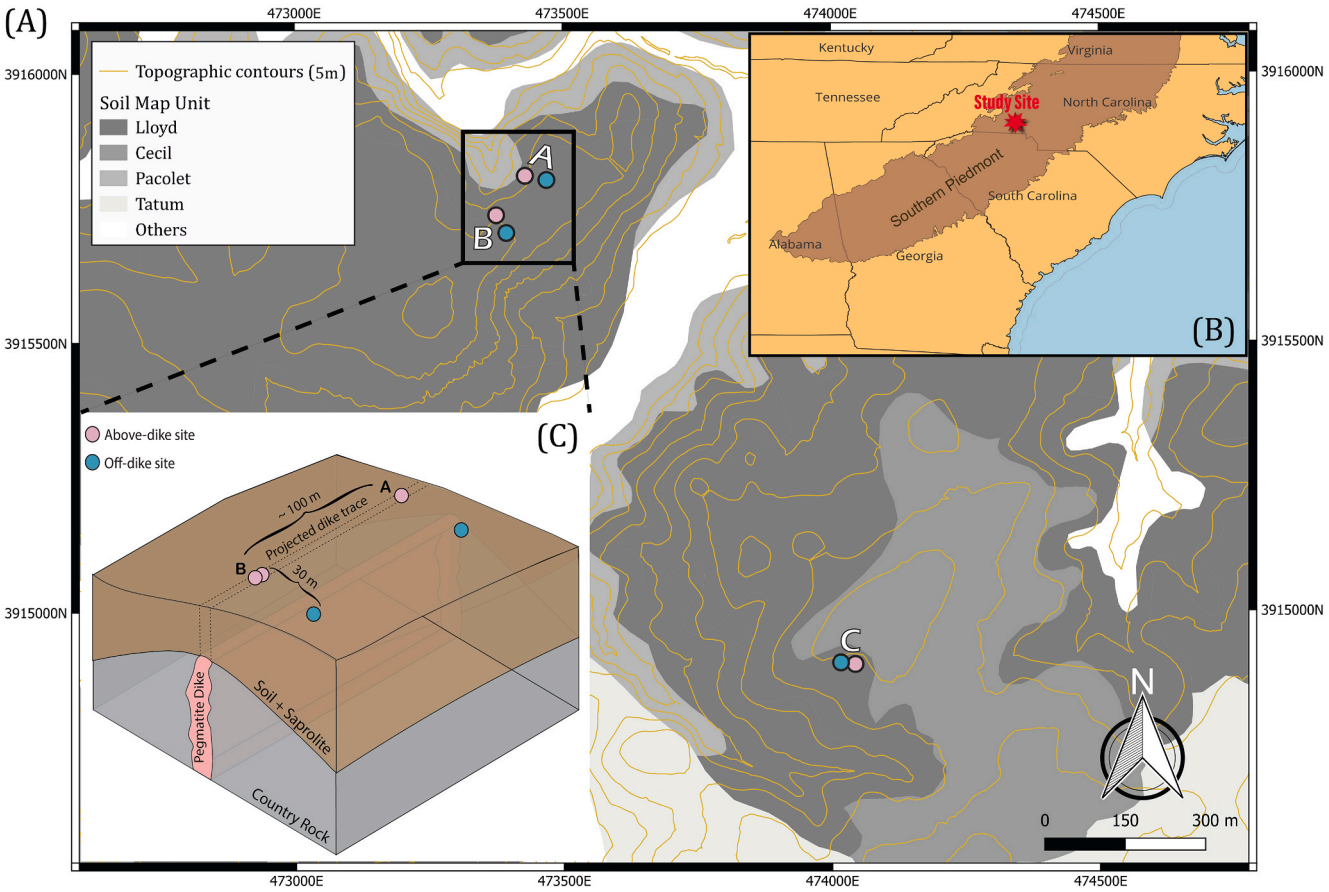


Fig. 2. (A) Map showing dominant soil map units of the study area with topographic contours (USDA-NRCS SSURGO database). Soil sampling sites (A-C) are indicated by dots, with above-dike sites shown in pink and off-dike sites in blue. The map boundary is labeled in UTM coordinates (zone 17 N). (B) Inset map showing the location of the study site (red star) within the southeastern United States and relative to the Southern Piedmont physiographic region. (C) Inset conceptual block diagram illustrates the geometry and projected trace of the Li-pegmatite dike relative to country rock, saprolite, and soils. The two sampling locations A and B are ~ 100 m apart, with off-dike cores collected ~ 30 m upslope from the above-dike sites. Diagram not to scale.

likely taken out of use since the mid-20th century and were subject to natural forest regeneration until a timber harvest around 2000, after which the sites regenerated naturally into their current mixed pine-hardwood stands (Fig. S1). In contrast, Site C was also an old field but has remained open agricultural land, with persistent field boundaries and field patterns indicative of tillage practices and is currently maintained as a hayfield at the time of sampling in 2025 (Fig. S2).

2.2. General soil characterization

After homogenization and subsampling, soil samples were air dried and passed through a 2-mm stainless-steel sieve. Soil texture was determined using a pipette method (Gee and Or, 2002) with ~0.02 M sodium hexametaphosphate (adjusted to pH 9.7 with Na_2CO_3) as dispersing agent. Exchangeable cations, defined as cations electrostatically adsorbed onto negatively charged soil surfaces and readily replaceable by other cations from the soil solution, were desorbed and extracted with 1 M NH_4OAc at pH 7 on a 1:10 mass of soil to volume of extractant basis (Hendershot et al., 1993). Metals associated with iron (Fe), manganese (Mn), and aluminum (Al) oxides and oxyhydroxides (hereafter referred to as oxides for simplicity), representing elements that have been weathered from primary minerals and retained in the secondary soil oxides (Bacon et al., 2012), were extracted with 1 M $HONH_2$·HCl (HA-HCl) in 1 M HCl at 90 ± 3 °C for 4.5 h (Wiederhold et al., 2007). This method yields results similar to dithionite-citrate-bicarbonate (DCB) extraction with soils from the southern Piedmont (Bacon et al., 2012). Soil pH was measured in 0.01 M $CaCl_2$, and exchangeable acidity determined by titrating extracts from 1 M KCl (Hendershot et al., 1993) with standardized NaOH to pH 8.2. Effective cation exchange capacity (ECEC) was calculated as the sum of exchangeable base cations (Na, Mg, K, and Ca) and exchangeable acidity. Effective base saturation (EBS) was calculated as the quotient of the sum of exchangeable base cations to ECEC. Soil carbon (C) was measured using a CHN automatic elemental analyzer (Thermo Scientific FlashEA 1112).

Soil mineral phases were determined by X-Ray diffraction (XRD) analysis using an Anton Paar XRDynamic 500 diffractometer with Cu Kα radiation (at Duke University's Shared Materials Instrumentation Facility, SMiF). Specific mineral phases in the bulk samples and of sand and silt grains and clay-size micelles were identified using powder diffraction by comparing 2θ peak patterns to the BGMN mineral database along with Profex 5.1 (Doebelin and Kleeberg, 2015). Sand-sized grains from soil samples were mounted in thin sections under 200 psi pressure and identified using a Leica DM2700 P petrographic microscope.

2.3. Total elemental concentrations

The total concentrations of Li and other elements (K, Rb, Sr, Na, Mg, Ca P, Fe, Al, Mn, Be, Zn, Ga, and Th) in all soil samples were determined by inductively coupled plasma mass spectrometry (ICP-MS) on a Thermo Fisher X-Series II instrument. Soil samples were pulverized using a ceramic mortar and pestle, and bedrock samples were processed using a ring mill. Homogenized powders were digested with an HF-HNO_3

mixture in closed Teflon vessels heated on a hot plate, following the procedures described by Wang et al. (2023) and Williams et al. (2024). This approach is based on established methods for acid decomposition of soil and geological materials (Chao and Sanzolone, 1992; Hossner, 1996). Analytical accuracy was evaluated through repeated digestion and measurement of National Institute of Standards and Technology (NIST) Standard Reference Material (SRM) 2711a, U.S. Geological Survey (USGS) granite G-2, and OREAS 753 LCT pegmatite. The SRM 2711a is representative of a soil matrix, and USGS G-2 and OREAS 753 have a lithologic similarity to the bedrock of the CTSB. All three standards have well-characterized, certified Li concentrations, and their analyses were within 15 % of the certified standard values for most elements of interest (Table S2).

2.4. Particle size fractionation

Bulk soil samples (< 2 mm) were dispersed and separated into sand (53 to 2000 μm), silt (2 to 53 μm), and clay (< 2 μm) fractions by sieving, sedimentation, and centrifugation (Whittig and Allardice, 1986; Deng et al., 2023). Briefly, soil slurries dispersed in 0.001 M Na_2CO_3 at pH 10 were wet sieved with manual agitation through a 53-μm stainless-steel sieve. The remaining slurry was separated into silt and clay fractions through a combination of sedimentation and centrifugation. Sand- and silt-sized particles were washed to remove Na_2CO_3, whereas the Na_2CO_3 content in the clay fraction was quantitatively estimated from the slurry volume after separation. The three fractions recovered were dried at 60 °C so as to minimize alteration of crystal structures.

2.5. Isotope analysis

Lithium isotope compositions were measured using a Nu Sapphire Multicollector ICP-MS at the Duke University SMiF. Lithium was separated with a column procedure following procedures outlined in Williams et al. (2026). Savillex PFA microcolumns with an inner diameter of 6.4 mm were filled to a height of 12.5 cm with 200 to 400 mesh AG 50 W-X12 resin. Lithium contents between 3500 and 4500 ng in each digested sample were prepared in 0.5 M HCl and were loaded onto the columns. Samples were eluted with 0.5 M HCl and collected in Savillex PFA vials. This was evaporated to dryness and then redissolved in 2 % v/v HNO_3 and diluted to 20 ppb Li/mL prior to MC-ICP-MS analysis. A few drops of H_2O_2 (~30 % w/w) were added to each sample during evaporation to remove dissolved organic matter. Eluted samples were regularly monitored to ensure complete recovery of Li from the columns and effective separation from Na.

Measured $^7Li/^6Li$ ratios were normalized to IRMM-016, a Li-isotope standard with an isotopic composition statistically identical to that of NIST L-SVEC (Qi et al., 1997), which was originally prepared from North Carolina spodumene ores from the CTSB (Flesch et al., 1973). Standard–sample bracketing was applied during each run (Millot et al., 2004). Values were reported as δ^7Li where $\delta^7Li = ([^7Li/^6Li]_{sample}/[^7Li/^6Li]_{IRMM\text{-}016}\text{-}1)*1000$. The accuracy of the measurement was assessed by measuring the International Association for the Physical Sciences of the Oceans (IAPSO) seawater standard. The measured value (29.93 ± 0.23 ‰, mean ± 2 se, n = 8) was within the analytical uncertainty of previously published values (Misra and Froelich, 2009; Jochum et al., 2005).

2.6. Mica analysis with LIBS

Laser-induced breakdown spectroscopy (LIBS) is a type of atomic emission spectrometry that can determine the multi-element chemistry of materials in any physical state. Geological applications of LIBS analysis, including soil analysis, are described in the reviews of Harmon and Senesi (2021, 2026), and Harmon (2024). To estimate the Li content of the soil mica fraction, muscovite $[KAl_2(AlSi_3)O_{10}(OH,F)_2]$ flakes were handpicked from the fine earth fraction (< 2 mm) of samples containing visible muscovite flakes that were sufficiently large for manual separation and LIBS analysis and analyzed for Li concentration using a SciAps Z-903 handheld LIBS instrument with a mica calibration developed following the procedure described in Harmon et al. (2025). The LIBS analysis of muscovite flakes employed a 4 × 3 grid (covering an area of approximately 1 mm × 0.7 mm) of laser shots, with four laser shots collected at each point and emission intensities for the 610.3 nm and 670.8 nm spectral lines averaged following two preliminary (non-recorded) 'cleaning' shots to minimize interference from oxide and organic coatings on the mica grains. Ten repeated measurements were performed on the surface of each mica grain and averaged to obtain the reported Li abundances and uncertainties.

2.7. Mass balance (τ) analysis

The mass transfer coefficient (τ) has long provided a useful approach to evaluate the mobility and redistribution of elements during weathering and soil formation (Brimhall and Dietrich, 1987; Brantley and Lebedeva, 2011). The calculation of τ is shown in Equation (1), where j is the element of interest; C is the elemental concentration; p represents the parent material; w refers to the weathered material; and i is the immobile reference element used for normalization. Positive τ values indicate net enrichment of an element relative to the parent material, whereas negative τ values indicate net depletion (loss) during weathering, with values approaching −1 reflecting near-complete loss.

$$\tau_j = \frac{C_{j,w}}{C_{j,p}} \frac{C_{i,p}}{C_{i,w}} \quad (1)$$

We conducted τ analyses to assess the pedogenic loss of Li in above-dike soils and weathering profiles. Thorium (Th) was selected as the immobile reference element because of its (i) conservative behavior in highly weathered soils, similar to that of Ti, Zr, and Nb (Braun et al., 1993; Braun and Pagel, 1994; Tsozué and Ndjigui, 2017; Beckford et al., 2023), (ii) similar concentrations in spodumene pegmatite and amphibolite that make it less sensitive to soil-mixing effects (Table S2), and (iii) higher analytical accuracy relative to Nb and Ti in our ICP-MS analyses.

2.8. Statistical analysis

All statistical analyses were carried out using the R software package (v 4.4.3; R Core Team, 2024). Two-tailed, unpaired t-tests (or Wilcoxon rank-sum tests when assumptions of normality were not met) were used to determine the difference of soil properties between above- and off-dike samples. Pearson's correlation coefficients (r) were computed as descriptive measures of the direction and strength of the observed associations among different soil properties. All analytical values were reported as means ± 2 standard errors (2se) along with coefficients of variation (CV) unless otherwise noted.

3. Results

3.1. General soil properties

Overall, the soil profiles exhibit properties characteristic of many highly weathered, acidic Ultisols found across the Southern Piedmont of the United States (Daniels et al., 1999), while also reflecting a localized lithologic influence of spodumene-bearing pegmatite, amphibolite, and metasedimentary parent materials underlying the CTSB. Like most of the Ultisols of the Southern Piedmont, CTSB soils have been highly eroded and chemically altered as a consequence of 19th to 20th century agriculture (McCracken et al., 1989; Richter and Markewitz, 2001). The soils are generally acidic (pH ranging from 4.0 to 6.4), exhibiting a decrease in pH with depth that is attributed to legacy influences from past agricultural liming and buffering effects of surface organic matter (Tables 1

and 2). Similar trends are observed in ECEC, which remains low throughout our soil profiles (between 0.8 and 4.2 cmol/kg) regardless of the parent material, except in surficial horizons enriched in organic matter. Values of EBS vary widely (from 23.9 % to 100 %) among profiles and with depth. EBS remains high throughout the shallow above-dike profiles at sites A and B, but decreases substantially with depth especially in saprolite C horizons in their off-dike counterparts. Despite the low ECEC, EBS remains near 100 % in both 5-m soil cores collected at site C down to about 2 m, below which it declines sharply.

Typically, above-dike soil profiles are significantly coarser in particle size than their off-dike counterparts, with an average soil sand content of 63 ± 5 wt% (CV = 20 %), reflecting the coarse-grained nature of the underlying pegmatite. Despite the overall coarseness of the above-dike soils, all soil profiles display a pronounced increase in clay content within the subsoil followed by a decrease at greater depth (in those that were able to be sampled to ≥ 2 m), highlighting the role of eluviation and illuviation in soil formation as well as the advanced stage of soil development. The increase in clay content in the subsoil generally meets the requirements for argillic and/or kandic horizons, and clay films are observed on soil peds. These Bt horizons are often dark red to rhodic in color, with moist hues of 2.5 YR and value and chroma ranging from 3 to 4 and 6 to 8, respectively, typical of the Cecil and Lloyd series. Shallow auger refusal was encountered at 50 and 125 cm in the above-dike profiles at sites A and B. Unlike Site C, these profiles do not reach well-developed saprolite, although an increasing number of lithoclasts is encountered near their bases. The coincidence of the abrupt auger refusal with still-increasing clay contents likely suggests the presence of resistant pegmatite corestones (boulder-sized blocks of relatively unweathered, solid rock that remain after surrounding bedrock and country rock have weathered away) within or near the weathering profile rather than undetached and unweathered bedrock.

3.2. Chemistry of total and extractable soil Li

Bulk soil Li concentrations (mean ± 2se) are substantially higher in above-dike soil profiles (1370 ± 480 mg/kg) than in their off-dike counterparts (212 ± 40 mg/kg) across all three sites (Fig. 3), with the highest concentrations (> 3500 mg/kg) observed in the shallow above-dike profiles at Sites A and B. Site C exhibits lower Li abundances relative to sites A and B. Consistent with the general elevation of Li in soils from the study area in CTSB reported by Harmon et al. (2025), measured soil Li concentrations for both above- and off-dike profiles greatly exceed the reported average for conterminous U.S. soils (Smith et al., 2013) and the Li abundances typical of soils elsewhere in the Southern Piedmont (Anderson et al., 1988; Rudnick et al., 2004) by one to two orders of magnitude.

Lithium displays large within-profile variability and heterogeneous depth distributions in above-dike soil profiles. Li concentrations in the

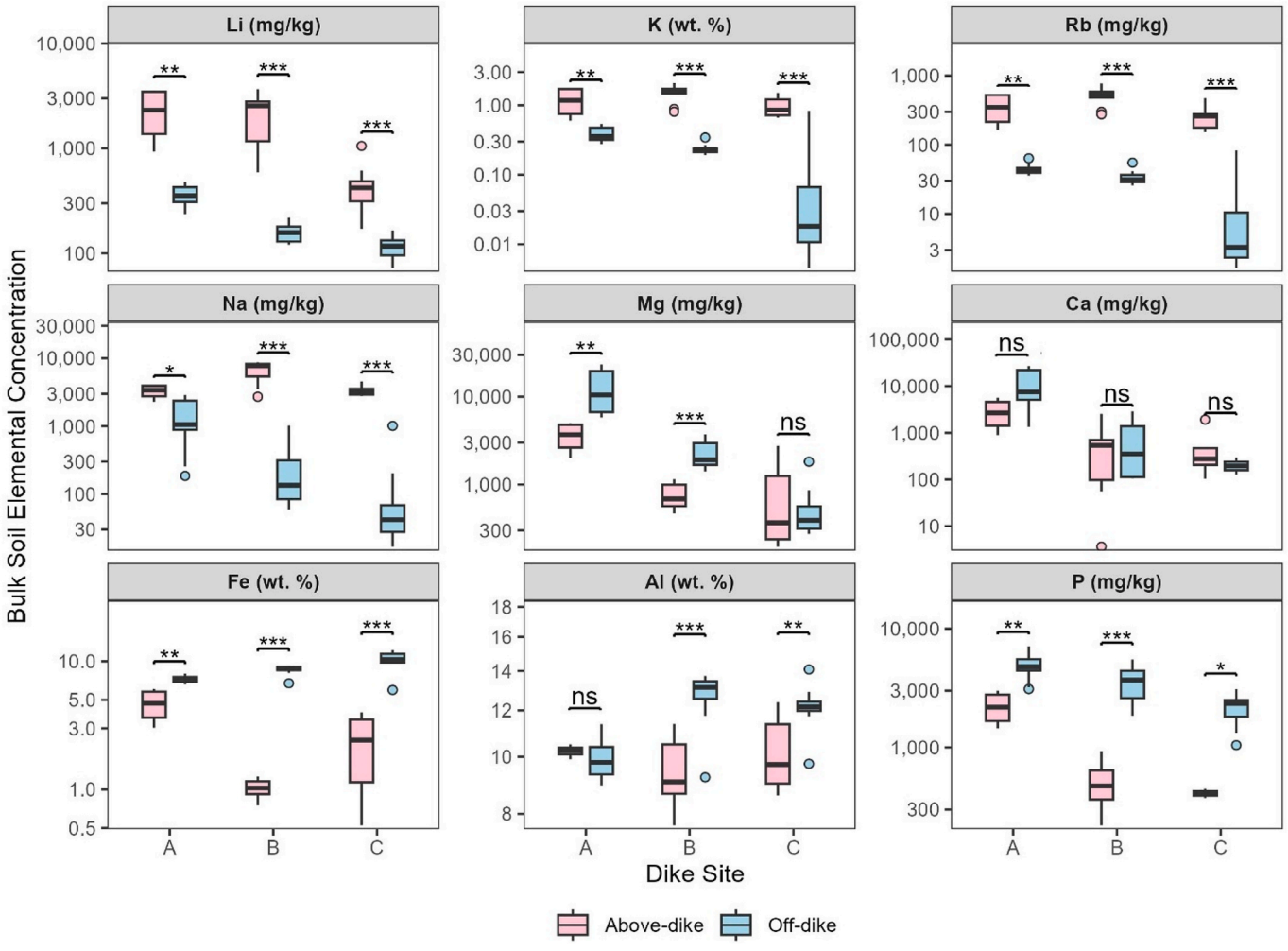


Fig. 3. Comparison of bulk soil elemental concentrations between above-dike (pink) and off-dike (blue) profiles across three sampling sites (A–C). Each panel shows boxplots of log-scaled elemental concentrations (Li, K, Rb, Na, Mg, Ca, Fe, Al, and P) measured in bulk soil samples, with units indicated in panel titles (mg/kg or wt. %). Boxes represent interquartile ranges; horizontal lines indicate medians; and whiskers extend to 1.5 × the IQR. Statistical significance between above- and off-dike groups at each site was evaluated using two-sided Wilcoxon rank–sum tests ($p < 0.05$ = *, < 0.01 = **, < 0.001 = ***, ns = not significant).

above-dike profile at Site A increase from 932 mg/kg at the surface to 3560 mg/kg at 50-cm depth, whereas in the 125-cm-deep above-dike profile 2 at Site B, they show a steady decrease from 2730 mg/kg at the surface to 591 mg/kg at 125 cm (Table 1). Li concentrations in the 5-m-deep above-dike profile at Site C are similar to those in the off–dike profile at the surface but increase gradually with depth, displaying relatively minor fluctuations before reaching 1060 mg/kg in the 4.5 to 5 m saprolite. In contrast, Li concentrations remain relatively uniform with depth in off-dike profiles (Table 2). These highly elevated Li signatures imply the pegmatitic origin of the above-dike soils and their significant retention of Li despite the element's high mobility during weathering.

3.2.1. Exchangeable Li

Chemical extractions provide a first approach for partitioning Li among its different soil fractions. Across all soils, exchangeable Li ranges from 0.0002 to 0.084 cmol/kg (0.01 to 5.83 mg/kg; mean ± 2se = 0.007 ± 0.0043 cmol/kg or 0.5 ± 0.3 mg/kg, CV = 220 %), constituting on average only 0.07 % of the total soil Li pool and 0.62 % of the total exchangeable cations (Table S3). The greatest amount of exchangeable Li is observed in the clay-rich subsoil of the above-dike profile at Site B, but it still represents only 0.5 % of the total soil Li. Overall, exchangeable Li is not correlated with soil clay content (r = -0.03), although a strong positive correlation is observed between exchangeable and total Li in off-dike soils (r = 0.80). These findings agree with earlier studies of southeastern U.S. soils that show exchangeable Li accounting for an insignificant fraction of total Li (Fig. 4A and C; Anderson et al., 1988).

3.2.2. HA-HCL extractable (HHE) Li

Oxide-bound or associated Li, which was estimated through a reductive HA-HCl extraction, averages 67 ± 15 mg/kg (CV = 53 %) in above-dike soils and 100 ± 30 mg/kg (CV = 90 %) in off-dike soils, representing a larger share of total Li than exchangeable Li (Tables 1 and 2). Despite no or only slight differences in HHE Li contents between above- and off-dike soils (Fig. 4 B), this fraction constitutes a substantially larger proportion of the total Li pool in off-dike profiles (mean = 31.0 %; range = 11.6 to 54.3 %) than in above-dike profiles (mean = 6.3 %; range = 2.1 to 22.0 %), a pattern consistent across all sites (Fig. 4 D). Our HA-HCl extraction recovered respective average proportions of 68 %, 53 %, and 21 % (Table S4) of the total Fe, Mn, and Al in bulk soils, comparable to the recovery range reported by Bacon et al. (2012). The HA-HCl extractable (HHE) Li is positively correlated with HHE Al (r = 0.73) among all soils and with HHE Mn within individual profiles at Sites B and C (r = 0.75 to 0.90), while showing no clear correlation with HHE Fe (Fig. S3A-C). Like DCB, the reductive HA-HCl extraction is more effective at extracting Fe and Mn oxides, with the recovered Al likely representing the amorphous or Fe-associated Al, along with Al dissolved by the acid matrix (Parfitt and Childs, 1988; McKeague and Day, 1966; Wiederhold et al., 2007). K recovery shows greater variability, typically < 10 % in above-dike soils but reaching higher values in off-dike profiles (Table S4). Together, the results indicate that the extraction primarily targeted secondary oxide phases rather than aluminosilicates such as the K-rich muscovite and feldspar. In general, HHE Li constitutes a small fraction of total Li in above-dike soils but represents a potentially important sink for Li when evaluating Li retention in off-dike soils. Despite the greatly elevated total Li in above-dike profiles, chemical extractions indicate that soil exchange sites and secondary oxides account for only a minor portion of it, pointing instead to crystalline aluminosilicate minerals, with structurally incorporated Li, as the primary hosts of soil Li signatures.

3.3. Associated element behavior

Bulk soil chemistry across a suite of elements reveals systematic differences between above- and off-dike profiles, highlighting contrasting parent materials and their strong geochemical influences on soil Li character. Along with Li, spodumene pegmatites are enriched in other incompatible elements, including potassium (K) and rubidium (Rb), that become concentrated during magmatic crystallization (Černý et al., 1985), both of which are enriched in above-dike soils. High sodium (Na) contents in above-dike soils likely reflect the presence of albite

Table 1
Total, exchangeable, and oxide-associated Li and other soil properties of above-dike soil profiles from CTSB.

Site	Hor	Depth, cm	Total Li, mg/kg	Exch Li, mg/kg	HHE Li, mg/kg	pH	Sand, %	Clay, %	SOC, %	ECEC†, cmol/kg	EBS§, %
Site A	A	0–12	**932**	**0.10**	**92.6**	5.3	52.0	10.1	5.7	14.7	99.3
	AB	12–25	**1560**	**0.11**	**107.0**	5.2	57.5	9.8	3.4	8.4	99.2
	Bt	25–38	**3450**	**0.46**	**114.0**	4.7	64.2	14.7	1.1	3.0	93.9
	Bt	38–50	**3560**	**0.99**	**127.0**	4.6	65.7	17.2	0.8	2.3	90.8
Site B (p1)	A	0–12	**3060**	**0.42**	**95.4**	5.0	75.0	3.5	–-*	3.8	98.4
	BA	12–25	**3670**	**1.12**	**78.6**	4.7	76.4	6.5	–-	1.5	91.6
	Bt	25–50	**2790**	**1.92**	**90.0**	4.4	74.9	10.2	–-	1.2	96.2
Site B (p2)	A	0–10	**2730**	**0.62**	**78.3**	5.6	77.9	2.3	4.2	12.0	99.5
	AB	10–20	**2550**	**0.51**	**83.2**	5.5	70.0	6.2	1.4	3.8	99.7
	BA	20–50	**1830**	**0.88**	**86.1**	5.2	72.1	8.1	0.3	1.5	99.9
	Bt	50–80	**1060**	**4.77**	**85.2**	4.0	68.7	16.8	0.2	1.4	73.8
	Bt	80–100	**1170**	**5.83**	**88.6**	4.1	70.1	19.3	0.2	1.3	83.4
	BCt	100–125	**591**	**3.43**	**130.0**	4.1	65.8	20.1	0.2	1.3	78.5
Site C	A	0–3	**171**	**BLK**	**22.4**	5.5	44.1	20.9	3.4	–-	–-
	BA	3–30	**186**	**BLK**	**22.8**	5.1	44.1	28.3	1.3	4.2	98.1
	Bt	30–50	**222**	**BLK**	**24.1**	5.7	39.2	37.4	0.5	2.8	100.0
	Bt	50–100	**506**	**BLK**	**21.4**	6.2	37.8	31.8	0.2	4.2	100.0
	BC	100–150	**615**	**BLK**	**22.4**	5.8	41.7	12.9	0.1	3.5	100.0
	BC	150–200	**380**	**0.03**	**51.0**	5.4	62.4	6.2	–-	2.5	100.0
	CB	200–250	**480**	**0.09**	**47.7**	4.7	67.1	10.1	–-	3.7	57.3
	CB	250–300	**467**	**0.06**	**56.1**	4.1	69.7	5.4	–-	1.7	96.3
	C	300–350	**351**	**0.04**	**31.4**	4.0	67.4	3.4	–-	1.3	92.8
	C	350–400	**356**	**0.05**	**21.6**	4.0	71.7	3.1	–-	2.3	37.4
	C	400–450	**475**	**0.03**	**37.1**	4.0	68.0	5.6	–-	3.1	30.3
	C	450–500	**1060**	**0.05**	**49.5**	4.0	69.2	5.6	–-	2.9	27.8

Notes: Hor—soil horizon; Exch—exchangeable; HHE—HA-HCl extractable; SOC—soil organic carbon; ECEC—effective cation exchange capacity; EBS—effective base saturation; p1—Profile 1; p2—Profile 2; BLK—blank: analyte indistinguishable from analytical blank.
* No data. Sample not analyzed, as the remaining samples were considered sufficiently representative.

Table 2
Total, exchangeable, and oxide-associated Li and other soil properties of off-dike soil profiles from CTSB.

Site	Hor	Depth, cm	Total Li, mg/kg	Exch Li, mg/kg	HHE Li, mg/kg	pH	Sand, %	Clay, %	SOC, %	ECEC, cmol/kg	EBS, %
Site A	A	0–8	**236**	**0.04**	**93.3**	4.6	43.9	20.6	2.7	6.8	93.7
	BA	8–25	**236**	**0.05**	**96.0**	4.1	34.3	31.1	0.7	3.0	55.0
	Bt	25–42	**343**	**0.14**	**183.0**	4.3	41.2	38.2	0.3	2.5	66.3
	Bt	42–60	**367**	**0.18**	**209.0**	4.5	49.1	30.4	–-	2.4	84.7
	BCt	60–80	**411**	**0.24**	**254.0**	4.6	64.4	17.2	–-	2.1	57.8
	BC	80–100	**450**	**0.33**	**292.0**	4.8	79.6	5.9	–-	1.0	74.1
	CB	100–120	**479**	**0.45**	**262.0**	4.7	82.5	1.3	–-	1.0	56.7
	CB	120–150	**433**	**0.46**	**261.0**	4.7	83.3	1.1	–-	0.9	53.1
	CB	150–175	**340**	**0.20**	**210.0**	4.2	58.9	5.6	–-	2.7	61.2
	CB	175–200	**298**	**0.19**	**220.0**	4.1	56.7	5.4	–-	3.0	57.7
Site B	A	0–8	**195**	**0.05**	**55.3**	4.4	44.0	21.7	3.6	4.0	88.2
	Bt	8–25	**123**	**0.04**	**29.3**	4.3	22.7	43.6	1.4	3.0	70.0
	Bt	25–42	**121**	**0.03**	**19.1**	4.3	11.5	47.1	0.6	2.6	68.3
	Bt	42–60	**152**	**0.03**	**17.5**	4.2	13.9	40.0	–-	2.9	53.4
	Bt	60–80	**122**	**0.14**	**22.5**	4.3	15.3	37.6	–-	0.9	47.9
	Bt	80–100	**151**	**0.02**	**43.6**	4.3	24.6	32.1	–-	1.0	49.8
	Bt	100–125	**168**	**0.08**	**56.7**	4.3	25.5	22.7	–-	1.3	59.5
	BCt	125–150	**164**	**0.06**	**69.6**	4.2	29.6	19.1	–-	1.1	26.8
	BC	150–180	**219**	**0.38**	**119.0**	4.1	49.9	9.7	–-	1.5	32.6
	BC	180–200	**184**	**0.05**	**97.8**	4.1	60.3	5.8	–-	1.3	35.2
Site C	BA	0–50	**165**	**0.01**	**33.0**	5.5	42.1	24.3	1.0	3.8	100.0
	Bt	50–100	**134**	**0.02**	**24.7**	6.4	38.4	27.3	0.2	3.5	100.0
	BCt	100–150	**130**	**0.04**	**28.6**	5.5	46.2	15.4	0.1	2.9	100.0
	BC	150–200	**125**	**0.09**	**62.3**	4.6	53.9	7.0	–-	2.0	96.8
	BC	200–250	**110**	**0.05**	**45.9**	4.3	47.1	6.6	–-	0.9	44.1
	CB	250–300	**95**	**0.09**	**22.7**	4.2	45.3	7.5	–-	1.4	28.0
	CB	300–350	**73**	**0.05**	**18.1**	4.1	38.7	9.0	–-	1.5	23.9
	CB	350–400	**96**	**0.10**	**27.2**	4.2	40.7	8.1	–-	1.2	34.1
	C	400–450	**96**	**0.05**	**44.8**	4.2	43.4	6.4	–-	0.8	39.5
	C	450–500	**146**	**0.04**	**68.2**	4.1	40.3	7.4	–-	1.3	26.8

Notes: Hor—soil horizon; Exch—exchangeable; HHE—HA-HCl extractable; SOC—soil organic carbon; ECEC—effective cation exchange capacity; EBS—effective base saturation.
* No data. Sample not analyzed, as the remaining samples were considered sufficiently representative.

[$NaAlSi_3O_8$], the predominant feldspar in the CTSB pegmatites (Swanson, 2012). The above-dike soils are relatively depleted in base cations and nutrient elements such as magnesium (Mg), calcium (Ca), and phosphorus (P), which are significantly higher in off-dike profiles derived from more mafic amphibolite and metasediment (Fig. 3). Details of the depth distribution patterns for K, Rb, Sr, Na, Mg, Ca P, Fe, Al, Mn, Be, Zn, Ga, and Th, are presented in Table S2. As is the situation for Li, the abundance contrast between above- and off-dike profiles at each site is generally preserved for most elements, but their concentrations can vary considerably across sites.

Correlations between Li and other elements yield further constraints on the nature of the soil Li reservoirs. Total Li shows the strongest positive correlations with total K (Fig. 5A; $r = 0.80$) and Rb (Fig. 5B; $r = 0.85$) across all soils. The two elements are themselves strongly correlated (Fig. 5E; $r = 0.94$), likely resulting from the substitution of Rb for K into muscovite and feldspar during pegmatite melt crystallization (Černý et al., 1985; Maneta and Baker, 2019), as well as the similar geochemical behavior of K and Rb during weathering and soil formation (Kronberg et al., 1987; Middelburg et al., 1988). Unlike K and Rb, the relationships of Li with Mg (Fig. 5C) and P (Fig. 5D) diverge between the above- and off-dike profiles, with the most pronounced positive correlations observed in off-dike soils ($r = 0.95$ for Mg; $r = 0.81$ for P). Likewise, the correlation between K and Mg ($r = 0.64$) is also evident only in off-dike profiles (Fig. 5F). For the HHE fraction, these relationships largely break down, with the HHE Li–K and Li-Mg correlations persisting only in off–dike soils at sites A and B (Fig. S3D-E). Considered together, the chemistry of the co-occurring elements supports the pegmatitic origin of elevated soil Li and implies a close association of Li with K- and Rb-bearing aluminosilicate phases in soils, with off–dike profiles reflecting Li reservoirs linked to more mafic parent materials.

3.4. Identifying Li in soil minerals

Mineralogical analysis provides a direct examination of crystalline phases and helps narrow down the potential Li-bearing minerals to further identify the mineral hosts of Li in soils. Soils derived from Li-pegmatite dikes are dominated by quartz [SiO_2], kaolinite [$Al_2Si_2O_5(OH)_4$], and muscovite, with feldspars [$(Ca,Na,K)(Si,Al)_4O_8$] present in the relatively shallow profiles at sites A and B (Figs. S4–S7). Quartz is a major constituent of both spodumene and common quartz-feldspar pegmatites of the CTSB and is present as an accessory mineral in the local country rock (Swanson, 2012). The high resistance of quartz to weathering leads to its abundance in well-developed soils even after most other primary silicate minerals (e.g. plagioclase) are largely dissolved during advanced stages of weathering (Calvert et al., 1980; Shaw et al., 2010). Kaolinite, as a common weathering product of feldspars in Ultisols and a stable secondary clay mineral, dominates the clay mineralogy of both above- and off-dike profiles, exhibiting a greater abundance in illuvial Bt horizons. In contrast, muscovite is more specifically associated with soils proximal to pegmatite lithology and is largely absent from off-dike soil profiles (Figs. S8–S10).

In the amphibolite-derived soil profiles at sites A and B, the appearance of basal reflections at 12.3 Å and 14–15 Å likely indicates the presence of an expandable phyllosilicate phase (e.g. smectite, vermiculite, or mixed-layer interstratifications), which becomes a significant component in the clay-rich subsoil and persists into the deeper saprolitic layers (Fig. S8 and S9). In addition, characteristic amphibole peaks are detected between 60 and 150 cm in the off-dike profile at Site A. The metasediment-derived profile at Site C shows no distinctive mineralogical features beyond the common kaolinite-dominated assemblage observed in the off–dike soils (Fig. S10).

The presence of muscovite in above-dike soils, and the higher-activity expandable clay mineral and amphibole phases in off-dike

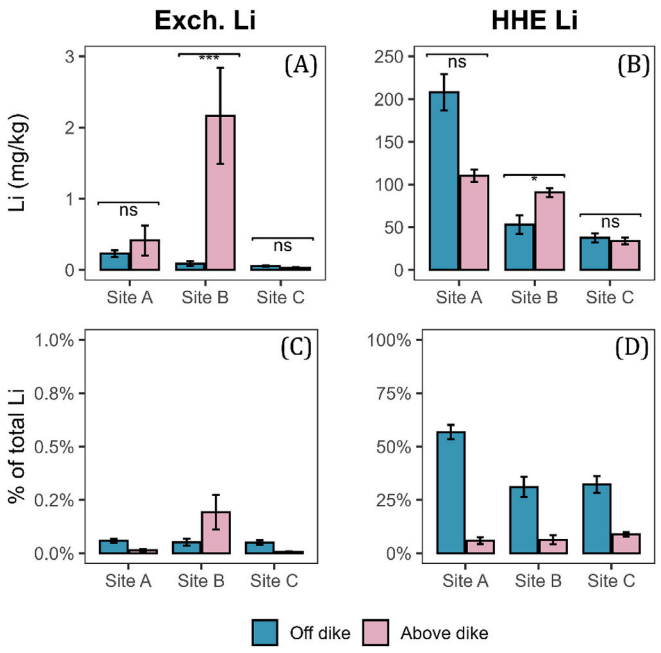


Fig. 4. Distribution of Li concentrations (mg/kg) among (A) exchangeable (Exch.) and (B) HA-HCl extractable (HHE) fractions in above-dike and off-dike soils across sites A-C, with statistical significance between above- and off-dike groups at each site evaluated using two-sided Wilcoxon rank–sum tests ($p < 0.05$ = *, < 0.01 = **, < 0.001 = ***, ns = not significant). (C) Same as (A), but showing exchangeable Li as a percentage of total Li. (D) Same as (B), but showing HHE Li as a percentage of total Li. Bars give group means and error bars denote ± 1 standard error (SE) across samples within each group. Detailed data, including the number of samples in each treatment group, are provided in Tables 1 and 2.

soils, reflect strong lithologic influence on soil minerology. In addition, several above–dike soils show weak peaks in the XRD patterns (Fig. 6A) that are consistent with trace amounts of spodumene, providing an important clue that guided our subsequent petrographic analyses.

3.4.1. *Size-fraction analyses*

XRD data on size-fractionated samples show strong association between soil mineral distribution and particle size. In a Li-rich surficial above-dike soil, primary minerals such as quartz and muscovite occur predominantly in the sand- and silt-sized fractions, whereas the clay-sized fraction is dominated by secondary minerals including kaolinite and the oxides (e.g. gibbsite [$Al(OH)_3$]; Fig. 6A). In contrast, kaolinite dominates all three size fractions in the subsoil of an off-dike profile (Fig. 6B). Total soil Li concentrations covary positively with sand contents (r = 0.54) and covary negatively with clay contents (r = -0.28) across all profiles (Fig. 7). The positive association between Li abundance and sand content is the most evident at sites A and B and becomes much weaker in the 5-m-deep profiles at Site C (Fig. 7A). This might be due to the greater sampling depth into the saprolite, which differs geochemically and pedogenetically from shallower soil horizons. Unlike sand, the covariation between clay and soil Li contents is much weaker and more variable among different profiles (Fig. 7B).

Chemical characterization of fractionated samples at Sites A and B shows the highest Li concentrations in the sand-size fractions (Fig. 7C). In soil samples spanning a range of depths and Li contents from the three above-dike profiles, Li concentrations in sands range from 1250 to 4950 mg/kg, disproportionately higher than in the finer silt and clay fractions and reaching up to seven times greater. The pattern becomes more variable at Site C, with the silt fraction having the highest Li contents in both subsoil and saprolite samples.

3.4.2. *Optical petrography of soil sands*

Optical petrography of thin-section grain mounts prepared from sand fractions of above-dike soils with elevated Li, ranging in sizes from coarse to fine sand, confirms the predominance of primary quartz and muscovite grains, with occasional feldspar (Fig. 8). Muscovite grains from the lower Bt horizon (1 to 1.5 m) in the 5-m above-dike profile at Site C are markedly smaller than those at Sites A and B (Fig. 8C and S9).

Most notably, petrography gives direct evidence of spodumenes in sand-sized soils. Spodumene is characterized and distinguished by an elongated and prismatic morphology, well-developed cleavages, low to moderate interference colors, and characteristic inclined extinction (Fig. 8A, B, and D). These spodumene grains are interpreted to be largely pristine, and their abundance is visually estimated from thin-section area, using standard comparison charts (Terry and Chilingar, 1955), to be approximately 5 to 10 vol% in the soil samples with the highest Li contents. Spodumene is common throughout the above-dike soils at sites A and B, whereas at Site C it is present, along with feldspar, in the deep saprolite (4.5–5 m), but absent from the overlying lower Bt horizon (1 to 1.5 m), where these minerals have likely become depleted through prolonged weathering dissolution (Fig. 8C and D).

3.4.3. *Li in soil muscovite and spodumene*

In general, the soil mineralogy across the CTSB points to two major Li carriers in above-dike soils- muscovite and, in soils with highly elevated Li, spodumene. Muscovite contains much lower (621 ± 502 mg/kg) Li than spodumene (Li = 3.0 ± 0.3 wt%; Curry et al., 2025) but still far more Li than the other major pegmatite minerals including K-feldspar, plagioclase, and quartz (Li < 70 mg/kg; Maneta and Baker, 2019; Curry et al., 2025; Harmon et al., 2025). LIBS analyses of hand-picked soil muscovite flakes in ten above-dike samples at sites A and B yield Li concentrations of 680 ± 120 mg/kg (CV = 29 %; Table S5), consistent with the range reported for muscovite in spodumene-bearing pegmatites from the region (Curry et al., 2025). This, in turn, further supports the presence of a Li-rich mineral phase in these soils, as muscovite alone cannot account for their exceptionally high bulk-soil Li concentrations (> 2500 mg/kg).

A component mass-balance calculation, using mean Li concentrations in muscovite and spodumene and assuming muscovite constitutes 20 to 30 wt% of the soil with ~60 mg/kg Li in all other phases, suggests that only ~7.5 wt% spodumene is required to elevate bulk-soil Li concentrations above 2500 mg/kg, which aligns with the 5 to 10 vol% trace spodumene abundance estimated from grain mounts. The abundance of spodumene in soils is substantially lower than the ~20 to 30 % modal abundance reported for spodumene pegmatites, which would correspond to an even higher proportion when expressed in wt% owing to the higher density of spodumene relative to other pegmatite minerals (Kesler, 1961; Hodges, 1983). This clearly indicates considerable loss of spodumene during weathering and soil formation.

3.5. *Weathering losses of Li*

Mass-balance considerations based on τ determination show that, despite the markedly elevated Li content in CTSB soils compared with non-pegmatite soils elsewhere, substantial Li has been lost from soils and regolith during weathering. A τ mass-balance analysis relative to the spodumene pegmatite (as the parent material), using Th as the immobile element, suggests an overall Li loss of 80.0 to 99.9 % (τ = -0.80 to −1.0) during pedogenesis in all above-dike soils (Table S2; Fig. 9). In the above-dike weathering profile cored to 5 m at Site C, a τ analysis relative to the deepest saprolite (Li = 1060 mg/kg) shows a full depletion profile, with $\tau_{Li,\ Th}$ decreasing almost steadily upward, approaching a value of −1 in the surficial horizons (Fig. 9). Such depletion patterns likely result from the removal of Li during spodumene dissolution, owing to Li's high mobility, and align with petrographic evidence for nearly complete spodumene loss in the lower Bt horizon (Fig. 8C).

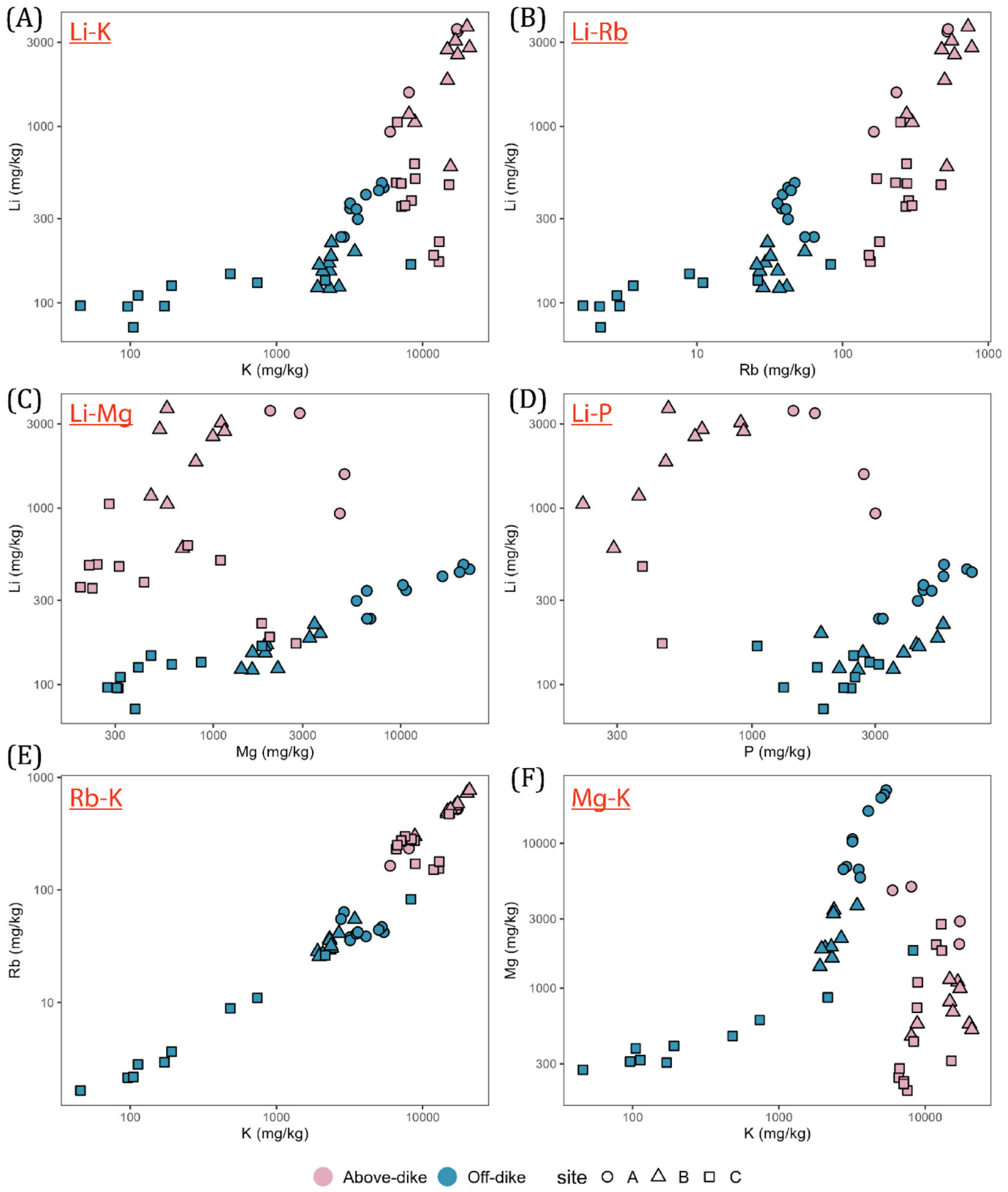


Fig. 5. Bivariate scatterplots of bulk soil elemental concentrations (in mg/kg) showing relationships among major elements of interest in soils above- and off-dike. (A) Plot of Li versus K. (B) Li v.s. Rb. (C) Li v.s. Mg. (D) Li v.s. P. (E) Rb v.s. K. (F) Mg v.s. K. Each point represents a bulk soil sample, with symbols distinguishing sampling sites (A–C) and colors indicating whether the profile is located directly above the pegmatite dike or off-dike upslope from it. All panels are log–log plots.

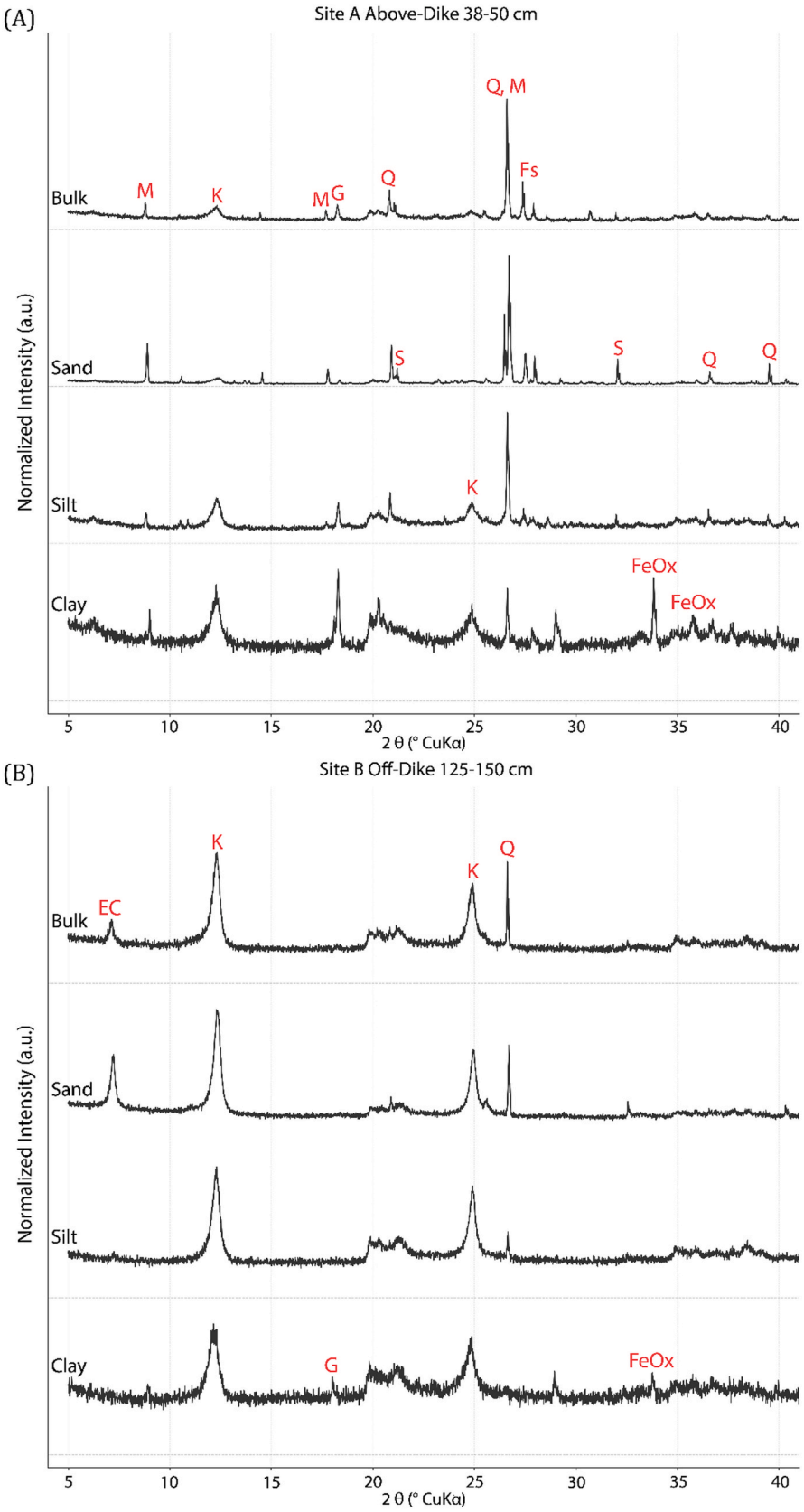


Fig. 6. X-ray diffraction patterns of the bulk, sand-, silt-, and clay-fraction soils from (A) 38–50 cm in above-dike profile at Site A and (B) 125–150 cm in off-dike profile at Site B. Samples have similar clay content, both from subsoil B horizons, and are representative of the above- and off-dike soil mineralogy. Peaks are labeled as quartz (Q), muscovite (M), kaolinite (K), feldspar (Fs), gibbsite (G), expandable clay (EC), Fe oxyhydroxide (FeOx), and spodumene (S). Measurements were obtained from powdered samples using CuKα radiation, with 2θ values shown along the x-axis. Each diffractogram was normalized to its maximum intensity, and the y-axis represents relative intensity in arbitrary units (a.u.).

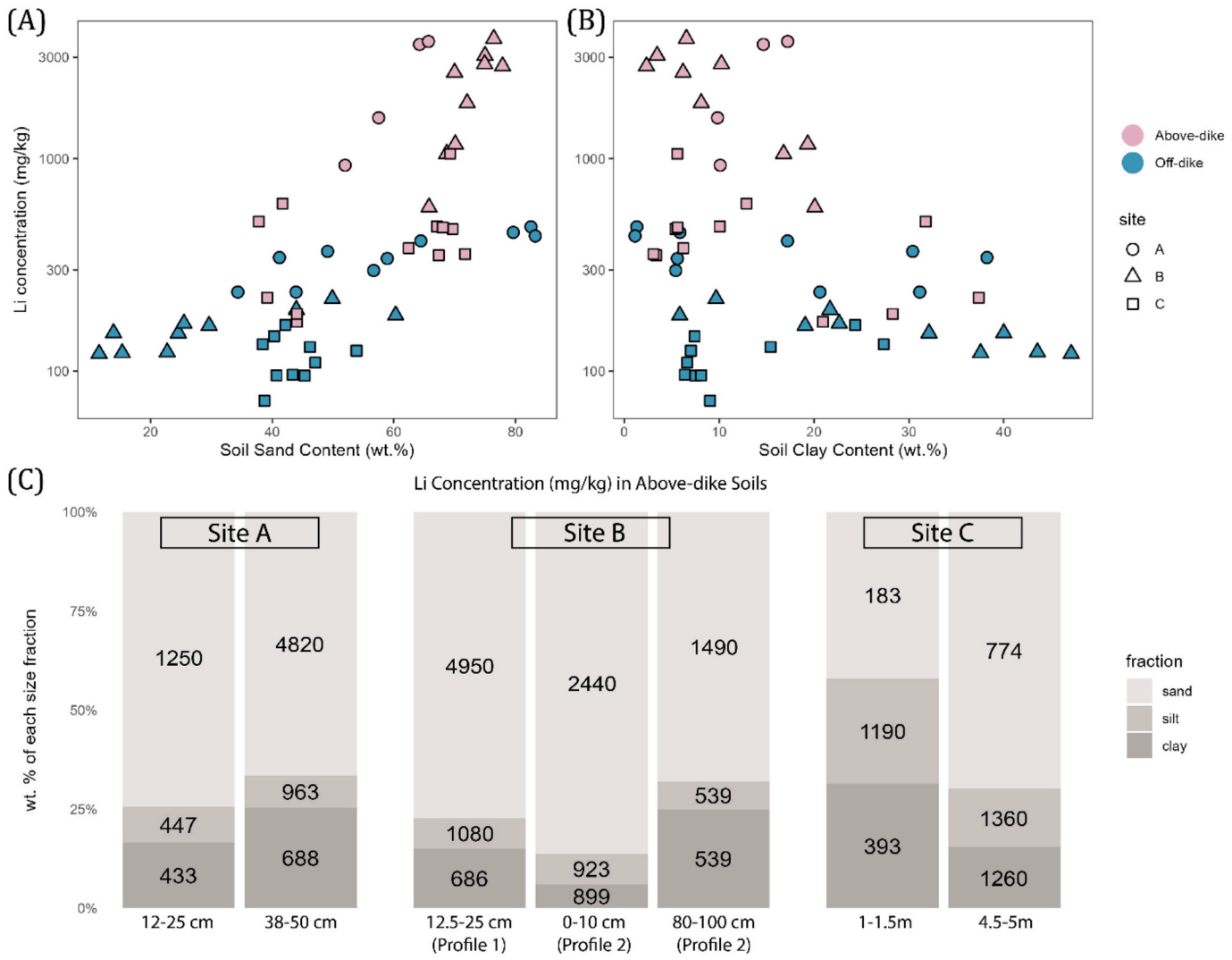


Fig. 7. Relationships between soil texture and Li concentrations across profiles at sites A–C. (A) Scatterplot showing bulk soil Li concentration versus sand content (wt.%). (B) Scatterplot showing bulk soil Li concentration versus clay content (wt. %). (C) Bar plot showing Li concentrations in sand, silt, and clay fractions for selected samples from above-dike profiles. Numbers denote Li concentrations (mg/kg) within each size fraction, and the vertical axis represents the wt.% of each size fraction.

3.6. *Li isotope composition of the soils*

Two bedrock samples collected from drill cores below soils representing two soil parent materials, spodumene pegmatite and amphibolite, yield similar Li isotope compositions (δ^7Li = -0.6 ‰), consistent with the ~ 0 ± 2 ‰ (1σ) average value for primary rocks and minerals of the upper continental crust (Teng et al., 2004). In contrast, δ^7Li values of bulk weathered soils and regolith samples from the three sites range from −13.69 to −0.93 ‰, revealing a marked isotopic difference between above-dike (−2.5 to −0.9 ‰, n = 6) and off-dike (−13.7 to −5.6 ‰, n = 5) profiles (Fig. 10).

At sites A and B, size-fractionated samples from the clay-rich subsoils of above-dike profiles have a consistent pattern of Li-isotope composition, with the sand fraction having the highest values (δ^7Li = -1.0 ‰ and −0.77 ‰), closely resembling the isotopic signatures of primary minerals, and the clay fraction characterized by substantially lower values (δ^7Li = -15.7 ‰ and −16.6 ‰), falling well within the range of bulk secondary minerals (Fig. 10; Pogge von Strandmann et al., 2020). The silt fraction has an intermediate Li-isotope composition (δ^7Li = -6.2 and −5.7 ‰). A similar trend is observed in the above-dike deep saprolite sample at Site C, but with a much smaller Li-isotopic variation among particle size fractions (δ^7Li = -0.8 ‰, −1.6 ‰, and −2.2 ‰ for the sand, silt, and clay fractions respectively). The lighter δ^7Li character of the silt and clay fractions may reflect the C–horizon saprolitic nature of the sample, in which the silt– and clay–sized fractions are likely dominated by fine–grained, unweathered primary mineral particles, with comparatively limited development of secondary clays such as kaolinite, relative to the overlying Bt horizons. For the three size-fractionated samples analyzed for Li-isotopic composition, mass balance calculations using the combination of δ^7Li values, weight percentages, and Li concentrations of each fraction recovered on average 94 % of the bulk δ^7Li value measured, providing a check on the internal consistency of our methods.

Li isotope composition in selected soil HHE fractions ranges from −18.4 to −7.8 ‰ (n = 5), representing the lightest values among all bulk and size-fractionated samples. No apparent difference is observed between above-dike and off-dike soils. The HHE fraction of the deep saprolite sample in the above-dike profile at Site C again exhibits the most ^{7}Li enriched isotopic signature (δ^7Li = -7.8 ‰) among HHE fractions, although it is notably isotopically lighter than all other δ^7Li values measured from this sample. The pattern of the HHE fraction being isotopically depleted is consistent across all samples. In the clay-rich Bt horizon (80 to 100 m) of the above-dike profile at Site B, the HHE (δ^7Li = -17.9 ‰) and clay-size fractions (δ^7Li = -16.7 ‰) both show remarkably negative isotopic values, which are consistent with previous

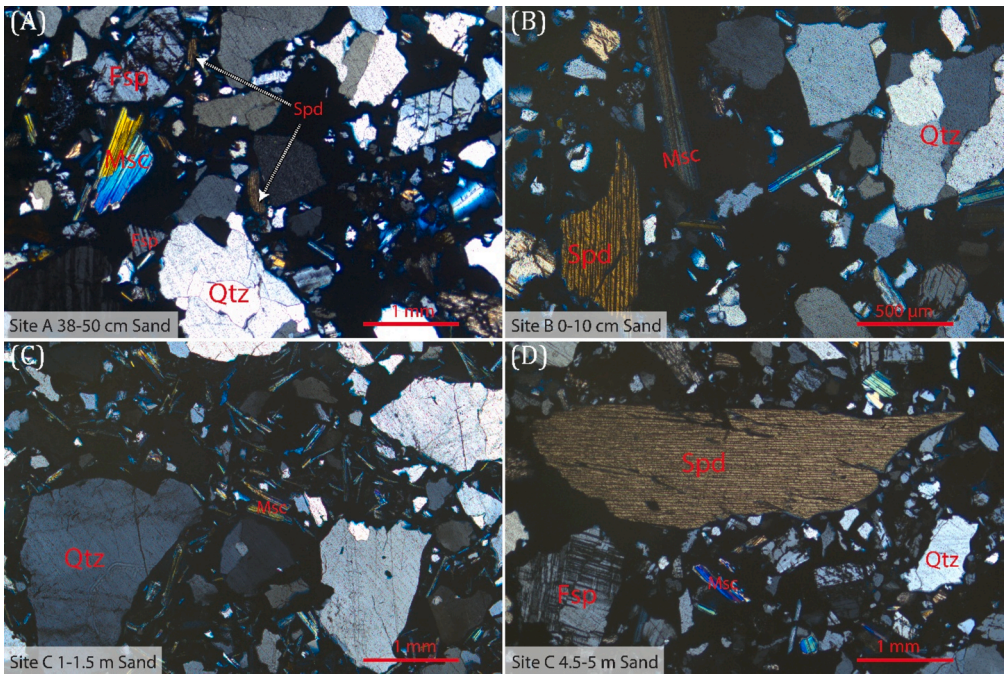


Fig. 8. Photomicrographs of the sand fractions of above-dike soils under cross-polarized light. (A) Site A (38–50 cm; Li = 3560 mg/kg) shows the general mineral assemblage of above-dike soil with highly elevated Li concentration, highlighting coarse quartz (Qtz) and muscovite (Msc), along with feldspar (Fsp) and minor amounts of small spodumene (Spd) crystals. (B) Site B Profile 2 (0–10 cm; Li = 2730 mg/kg) features a well-preserved, large spodumene grain surrounded by quartz and muscovite. (C) Site C (1–1.5 m; Li = 615 mg/kg) shows predominance of quartz and muscovite. Muscovite grains are markedly smaller than quartz, and no spodumene or feldspar were observed. (D) Site C (4–4.5 m; Li = 1060 mg/kg) features large spodumene and feldspar crystals identified in the saprolite in addition to muscovite and quartz. Scale bars: 1 mm in (A), (C), (D) and 500 μm in (B).

δ^7Li measurements of Li sorped onto Fe oxides (Zhang et al., 2025). The δ^7Li measurements reported in this study have a mean two standard error (2se) analytical precision of ± 0.11 ‰ (Table S6).

4. Discussion

4.1. The fate of Li during pedogenesis above a Li-pegmatite dike

Lithium isotope analysis provides an important constraint to our understanding of soil development in the CTSB by differentiating Li hosted in primary versus secondary phases, as δ^7Li compositions are sensitive to the isotopic fractionations during release of Li from primary minerals and its subsequent incorporation into secondary clays during weathering and soil formation (Pogge von Strandmann et al., 2020). The relatively ^{7}Li-enriched isotopic composition of above-dike soils, which approaches that of the primary rocks and minerals (Fig. 10), corroborates other findings from this study: (i) the strong association between Li content and the soil sand fraction, where relic primary mineral grains are most abundant (Fig. 6A, 7, and 8); (ii) the strong positive covariations between bulk soil Li content and both K and Rb abundance (Fig. 5A and B); and (iii) the negligible exchangeable Li pool and the generally small (<10 %) contribution of the HHE Li fraction (Fig. 4). Collectively, these observations suggest that Li signatures in above-dike soils are primarily driven by the persistence of Li-bearing primary minerals that have survived weathering.

As soils are produced from the weathering of the parent rock, Li-rich primary mineral grains are progressively incorporated into the developing regolith, carrying their Li signatures into the overlying soils. The occurrence of less weathering-resistant minerals (relative to quartz and muscovite), such as spodumene and plagioclase in several surficial soil horizons at sites A and B, is noteworthy given the intense and prolonged weathering regime across the Southern Piedmont. We attribute this to the relatively shallow emplacement of the pegmatite dike at these sites. Compared to the deep weathering profile at Site C where true pegmatite saprolites are recovered, the shallow auger refusals here suggest the likely presence of less weathered materials such as pegmatite corestones that supply fresh primary minerals directly to the overlying soils during weathering. In addition, spodumene-quartz intergrowths are widely documented in Li-pegmatites worldwide including at the CTSB (Swanson, 2012; Brennan et al., 2024; Goodenough et al., 2025) and could contribute to the persistence of spodumene in the regolith through protection by weathering-resistant quartz. However, because petrographic observations were made on soil grain mounts rather than intact rock thin sections, potential mineral intergrowths could not be assessed directly.

Here, we propose a general pathway for the fate of Li in soils derived from Li-pegmatite: once weathering releases Li from primary minerals, it is preferentially leached from the system (Fig. 9). This is a consequence of: (i) the extremely low affinity of Li for soil electrostatic exchange sites compared with cations that possess larger ionic radii and higher valence charges (McBride, 1994; Robinson et al., 2018), (ii) the dominance of secondary mineral phases by kaolinite, whose structural simplicity limits its capability to incorporate Li (Rudolph et al., 1995; Brady and Weil, 2017; Li and Liu, 2020), and (iii) limited scavenging by Fe, Mn, and Al oxides. Under such conditions, relic Li-rich primary mineral grains that persist in the soil matrix become the dominant contributors to the observed soil Li signatures. Therefore, rather than being actively and significantly retained by secondary phases, the soil Li signature is primarily a function of weathering and pedogenic loss.

4.2. Li enrichment in soils derived from country rock

Given the amphibolite parent material, the occurrence of expandable clay minerals in off-dike soils together with the weakening or disappearance of 10-Å mica peaks suggests that these phases may represent alteration products of primary biotite, such as vermiculitized biotite or mixed-layer biotite-vermiculite. Their occurrence along with kaolinite in the sand-sized fraction (Fig. 6B) is consistent with their formation

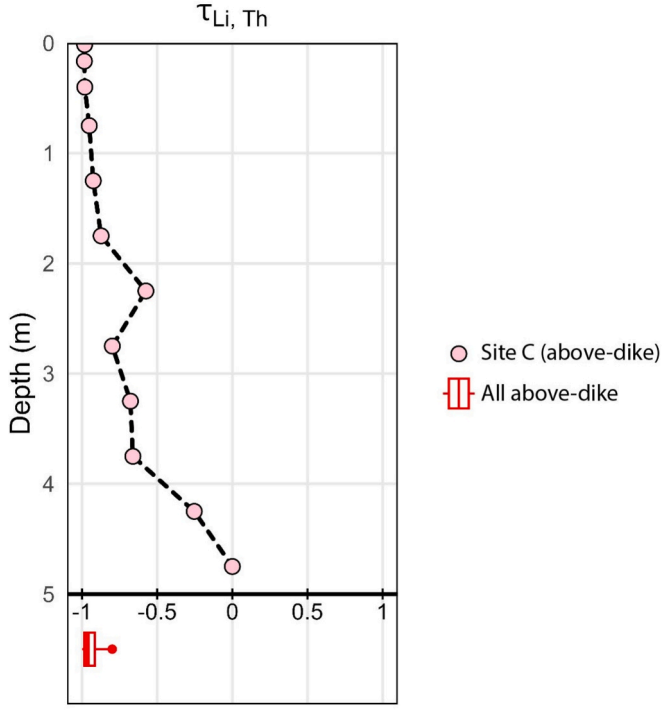


Fig. 9. Mass transfer coefficient of Li normalized to Th ($\tau_{Li,\ Th}$) for above-dike soils. The upper panel shows the depletion profile of $\tau_{Li,\ Th}$ from 5 m to soil surface in the above-dike profile at Site C, referenced to saprolite at 4.5 to 5.0 m depth. The lower panel shows a box-and-whisker summary of $\tau_{Li,\ Th}$ across all above-dike soils, referenced to the spodumene pegmatite bedrock. The box indicates the interquartile range, the central line marks the median, and whiskers extend to 1.5 × the interquartile range. Li is highly depleted in all soil samples relative to the pegmatite bedrock, with an overall loss of 80.0 to 99.9 % during pedogenesis.

through alteration of coarser primary mineral grains, with the weathering products retained as sand-sized pseudomorphic crystals (Rebertus et al., 1986; Rebertus and Buol, 1985). Biotite in metamorphic rocks can contain Li and may become further enriched through metasomatic interactions with Li-rich granitic-pegmatitic sources (up to 560 ppm Li on average proximal to Li-rich pegmatite intrusions; Xiao et al., 2026). Its alteration products are therefore likely important Li carriers in off-dike soils, as implied by the strong positive correlations between total Li and K, Rb, and Mg (Fig. 5A-C, F). Unlike muscovite, biotite is less resistant to weathering and almost never occurs in its pristine form in surface soils of Piedmont Ultisols (Rebertus et al., 1986). Through weathering-driven modifications, including interlayer expansion, Fe oxidation, and enhanced reactivity at edges and wedge-zone sites (Fordham, 1990; Banfield and Eggleton, 1988), the Li-isotope signatures of primary biotite can be mixed and become lighter with partial alteration and secondary clay formation (i.e. interstratification), depending on the extent to which ^{7}Li is preferentially lost during weathering (Pogge von Strandmann et al., 2020). Such processes, together with Li associated with secondary oxides, may have contributed to the intermediate Li–isotope compositions observed in the off-–dike soils.

4.3. Nature of the HHE fraction and the secondary Li pool

Fe, Al, and Mn oxides are well recognized as important scavengers of trace metal(loid)s, including Li, through surface complexation, structural incorporation, and physical occlusion during oxide formation (Jenne, 1968; Besserguenev et al., 1997; Lion et al., 1982; Negra et al., 2005; Kim and Grey, 2010; Grangeon et al., 2020; Li et al., 2024). As is evident from the recovery rates of Fe, Mn, and Al, the positive correlations between HHE Li and HHE Mn and Al (see Section 3.2.2 and Fig. S3), and the isotopically lightest δ^{7}Li signature of the HHE fraction, our HA-HCl extraction effectively targets Li associated with these secondary oxides. The similar absolute HHE Li contents (Fig. 4 B) in above- and off-dike soils suggest that the oxides retain comparable amounts of Li in both settings. The much smaller relative contribution of the HHE fraction in above-dike soils therefore primarily reflects their substantially larger total Li pool due to the presence of Li-rich primary phases

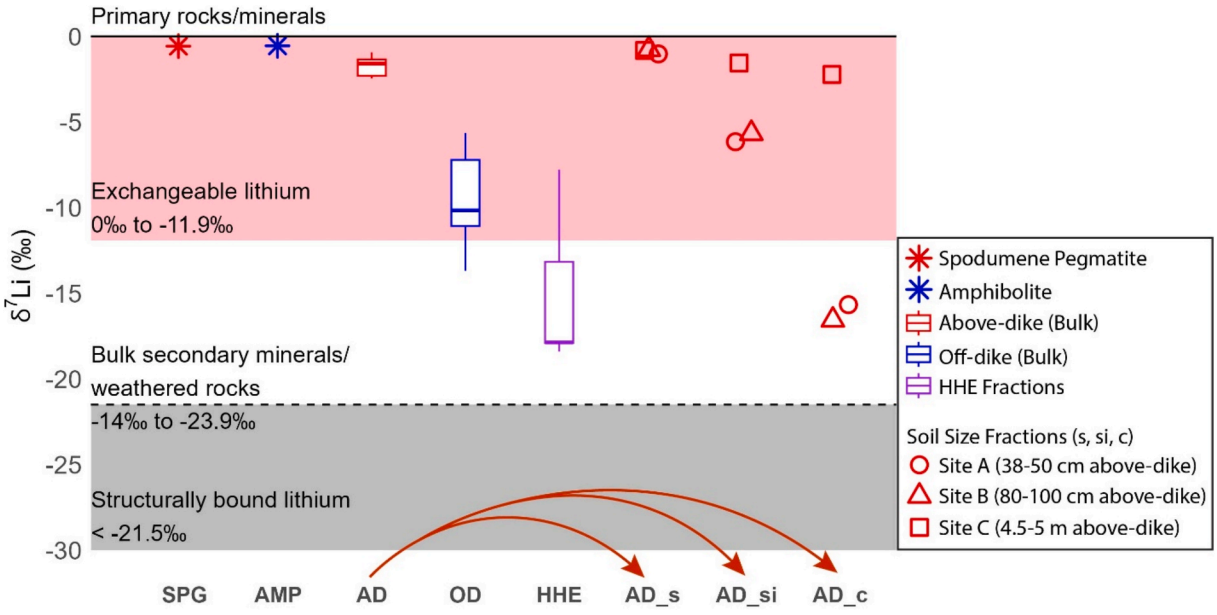


Fig. 10. Lithium isotope composition (δ^{7}Li, ‰) of bulk soils and size and chemical fractions from above- and off-dike profiles at Sites A–C. SPG—spodumene pegmatite; AMP—amphibolite; AD—above-dike bulk soils; OD—off-dike bulk soils; HHE—HA-HCl extractable fractions; s—sand; si—silt; c—clay. Reference δ^{7}Li ranges are adapted from Pogge von Strandmann et al. (2021): ~0 ± 2 ‰ for primary rocks and minerals, 0 to –11.9 ‰ for exchangeable Li, –14 ‰ to –23.9 ‰ for bulk secondary minerals and weathered rocks, and values below –21.5 ‰ for Li bound to the structure of secondary minerals. Bulk secondary minerals represent the combination of exchangeable and structurally bound Li and therefore fall between these endmembers. Analytical uncertainties are reported in Table S6.

associated with spodumene pegmatites, rather than differences in Li scavenging by pedogenic oxides.

Nonetheless, the HHE fraction is likely not exclusively derived from the oxide pool, especially in off-dike soils, as the acid matrix of the extractant might partially dissolve more labile phyllosilicates such as biotite and its derivatives. The partial dissolution of altered biotite during extraction is suggested by the positive correlations between HHE Li and HHE K, Rb, and Mg (Fig. S3C-E), indicating that a portion of Li is co–released with these elements. This is expected given the much higher leachability of biotite in acid conditions (Snäll and Liljefors, 2000) when compared to other primary silicates, especially when its structure has been weakened by alteration. In addition, phosphate minerals are known to occur in both primary and secondary forms in accessory amounts mainly within CTSB pegmatites (Hodges, 1983; Swanson, 2012) and can carry Li and contribute Li under leaching conditions (Williams et al., 2024). These phosphate minerals (e.g. fluoroapatite [$Ca_5(PO_4)_3F$]) are susceptible to weathering, and if still present in their original forms in the soils, would be readily dissolved by the acid-matrixed HA-HCl extractant. However, the substantially higher P abundances in off-dike soils at all three sites (Fig. 3), rather than in above-dike soils derived from phosphate-hosting pegmatites, suggest that primary phosphate minerals have likely been weathered out and P lost from above-dike profiles; while off-dike soils, having more abundant Fe-oxide phases, can potentially retain and scavenge more P released during mineral weathering as well as P added through historic fertilization (Richter et al., 2006). Therefore, the Li-isotope composition of the HHE fraction likely includes minor contributions from other labile phases, rather than representing a purely oxide-bound Li pool.

In addition to exchangeable and HHE Li, soil organic matter may also contribute to the secondary Li pool, as Li participates in biological cycling through plant uptake and litterfall (Robinson et al., 2018). Nonetheless, the natural concentration of Li in plants and organic matter (Miletić et al., 2024) is likely extremely low relative to that of the Li-bearing minerals in the soils we studied. Only a very small fraction of the total soil Li occurs in the exchangeable pool (Fig. 4 C), indicating limited bioavailability. Furthermore, organic matter contents in the studied mineral soils are generally < 4 % at the surface and become negligible below the A horizon (Tables 1 and 2). Consequently, Li associated with vegetation and soil organic matter is expected to represent an inconsequential fraction of the total Li inventory relative to mineral-hosted Li in these profiles.

4.4. Processes controlling Li distribution in soil and weathering profiles

4.4.1. Soil mixing

Though we have treated above- and off-dike soils as distinct, weathering products derived from different sources can co-exist within a single profile as both pegmatite dikes and country rocks weather together. Pedoturbation, including bioturbation by tree roots and soil fauna, redistributes Li-bearing mineral grains and weathering products within and among soils, particularly within the biologically active near-surface soils and rooting zones (Roering et al., 2002; Jungers et al., 2009). Such materials can also be mixed through geomorphic processes such as soil creep (McKean et al., 1993; Roering et al., 2001; Richter et al., 2020) and aeolian transport and deposition (Markewich et al., 2015). For example, Sirbescu et al. (2025) noted lithoclast transport as a potential mechanism underlying the enrichment of pegmatite-associated elements in soils developed on adjacent country rocks. Mixing curves have been demonstrated as a useful approach to assess the degree of mixing between two parent material end members (Hall et al., 2025). Here, we calculated hypothetical mixing curves between spodumene pegmatite and amphibolite (using the averaged bedrock compositions from Hall et al. (2025) and this study as end members) at sites A and B and between pegmatite and metasediment (simulated using the deepest saprolite sample in off-dike soil profile) at Site C, based on their respective K/Rb and Rb/Sr values (Fig. 11), elemental pathfinder ratios that effectively distinguish the above– and off–dike soils (Fig. S12; Hall et al., 2025; Harmon et al., 2025).

All soil samples fall along or near the hypothetical pegmatite-amphibolite mixing curve at both sites A and B, indicating that the soils represent mixtures of the weathered products of these two end members. Above-dike soils show > 50 % contribution from pegmatite-weathered materials with most exceeding 90 %, making them readily distinguishable from off-dike soils, in which the pegmatite share is < 25 % and typically around or below 10 %. At Site A, mixing increases toward the surface in both above-dike and off-dike profiles, reaching roughly 25 to 40 % in near-surface soils, where soil materials are more susceptible to erosional and colluvial processes (Fig. 11A). This is further supported by mineralogical data, as amphibole-like grains were identified near the surface of the above-dike profile at Site A in both XRD patterns and petrographic observations (Fig. S4 and S13). Such a trend is not as evident at Site B, where mixing remains weak in both profiles, potentially due to the gentler slope gradient at this site (Fig. 11B).

Strong mixing occurs in the surface horizons of the above-dike profile at Site C, where the soils in the top 1.5 m display < 25 % pegmatite signatures and are barely distinguishable from those off-dike (Fig. 11C). This may result from both the deeply weathered nature of the profile at Site C, which allows for a longer period of mixing, as well as its continued agricultural use that can facilitate erosion. In contrast, deeper samples from this profile show very strong pegmatite signatures, exceeding the average values of the pegmatite end member used in the mixing calculations, though still falling along the extension of the mixing curve. We interpret this as reflecting local variability in pegmatite composition (Griffitts, 1954; Kesler, 1961). In general, greater degrees of mixing in above-dike profiles is consistent with their downslope position relative to the soils off-dike, allowing material from upslope to be incorporated through gravity-driven transport.

4.4.2. Eluviation-illuviation

Eluviation and illuviation, as key pedogenic processes in well-developed, clay-rich Ultisols, can potentially influence the depth distribution of Li. By translocating fine, clay–sized particles downward from the surface, these processes alter the particle–size distribution by leaving a relative enrichment of the coarser, sand–sized grains near the surface. For example, in the 125-cm-deep above-dike profile at Site B, bulk soil Li concentrations covary strongly with sand content (Fig. 7A), being the highest at the surface and decreasing steadily with depth as the proportion of sand and coarse silt declines. A similar pattern is also observed in the off-dike profile at Site B. Note that the decreasing trend of Li with depth is only observed at Site B, where surface mixing is minimal (Fig. 11). Products of translocation may have been masked or overprinted by mixing processes at the other sites.

4.4.3. Weathering and the soil particle conveyor

Weathering itself shapes soil Li distribution as it releases Li from the primary mineral structures and eventually leads to the loss of Li from the soils (see section 4.1). A deeper profile such as that at Site C displays more pronounced vertical weathering gradients, wherein particles nearer the surface have undergone more prolonged weathering, resulting in greater Li depletion (Fig. 9). Thus, weathering and surface mixing of off-dike material likely acted together to produce the relatively low Li concentrations at the surface in the above-dike profile at Site C. Moreover, weathering offers an alternative, non-exclusive explanation to the covariation between soil Li concentrations and sand contents, as it drives both the loss of Li through leaching and the reduction of particle size in soils through processes like comminution (Rebertus and Buol, 1985; Buol et al., 2011), which may explain the shift in Li enrichment toward finer particle-size fractions at Site C (Fig. 7C). Alternatively, this pattern may simply reflect differences in pegmatite bedrock texture among the study sites.

Much like the soil Li signatures, vertical compositional heterogeneity

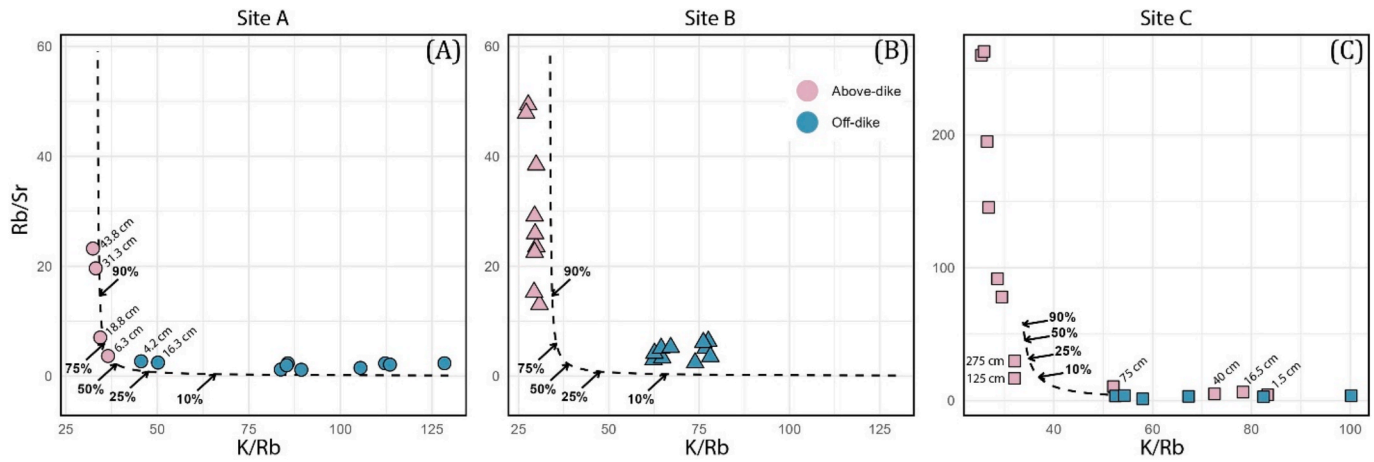


Fig. 11. Mixing model between spodumene pegmatite and country rock using K/Rb and Rb/Sr ratios at sites A-C. (A) Profiles from Site A (above- and off-dike) plotted against the hypothetical mixing curve (dashed line). Endmembers represent the mean value of K/Rb and Rb/Sr in sampled whole-rock Li-pegmatite and amphibolite. The percentage of pegmatite contributions is labeled along the curve, with arrows pointing to key increments (10 to 90 %). (B) Profiles from Site B on the same mixing curve. (C) Same mixing framework applied to Site C profiles, with the composition of metasedimentary country rock simulated using the 4.5 to 5 m saprolite in the off-dike profile. Soil sample depths (cm) are shown for selected samples with intermediate to high degrees of mixing.

in the bedrock can be carried into the soil and weathering profiles by the particle conveyor, contributing to the depth-dependent variability in soil properties. Consequently, the Li distribution observed in a weathering profile may partly reflect heterogeneity, or the uneven distribution of elements, in the original pegmatite dike or country rock, rather than pedogenic processes alone. However, unlike many other pegmatites that exhibit significant heterogeneity (London, 2018), soils derived from CTSB pegmatites are less likely to reflect such effects because these pegmatites typically display little internal compositional zoning (Swanson, 2012; Curry et al., 2025). In the end, soil formation is a complex process that involves both pedogenic processes and lithologic controls that collectively shape the distribution of Li within soil and weathering profiles.

4.5. *Implications for soil prospecting*

In this study, we used a profile-based approach to compare above- and off-dike soils at a spacing of 30 m, an interval that is similar to those used in recent Li-pegmatite soil prospecting studies (Hall et al., 2025; Harmon et al., 2025; Pierangeli et al., 2025). Within this framework, our results indicate the potential of three bulk soil geochemical tracers for distinguishing above-dike profiles from their off-dike counterparts: (i) total Li concentration, (ii) K/Rb, and (iii) Rb/Sr in bulk soils (Fig. S12).

A discrepancy between our results and those reported by Harmon et al. (2025) and Hall et al. (2025) concerns the performance of bulk soil K/Rb as a Li-pegmatite pathfinder, which both studies found to be ineffective. This difference may arise from two factors: First, our work relies on depth-resolved sampling from the soil surface downward through the entire profile, rather than using composite samples from a specific depth interval (e.g. topsoil or the subsoil Bt horizon). This allows us to account for the mixing and pedogenic processes that could redistribute geochemical tracers, blurring or homogenizing signals in composite samples. For example, at Site C, where surface signatures of pegmatite are largely obscured, a full-profile approach allows us to detect the geochemical differences that only become apparent at greater depths (> 1 m). Secondly, the influence of surface mixing from hillslope processes is intentionally minimized in this study by selecting only soil profiles located upslope from the above-dike profiles to represent the off-dike sites. In real-world settings, soil geochemical signatures should be interpreted with consideration of the potential for soil mixing at each site. As observed at sites A and C, mixing with materials potentially derived from upslope may attenuate the Li-pegmatite signature in above-dike soils (Fig. 11A and C). Conversely, by the same reasoning, redistribution of pegmatite-derived materials may impart this signature to surface layers of off-dike soils downslope from the source. In that case, a surface-soil anomaly identified during exploration might reflect material transported from upslope rather than directly overlie its bedrock source. Further testing is needed to evaluate this possibility and determine whether such mixing signals can be used to predict the locations of upslope or nearby Li-pegmatite sources.

Thus, our findings highlight the importance of sampling depths in Li soil prospecting. Given the vertical variability of geochemical tracers, it would be ideal to collect weathering profiles and characterize soil chemistry at multiple depth ranges throughout the profile to capture the most well-pronounced differences between off-dike and above-dike soils. Even just below 1 m, the difference between pegmatite and country-rock signature becomes clearly expressed across all three of our CTSB sites, including Site C, where dike emplacement is much deeper. Reaching depths of 1.5 to 2 m is generally feasible with a standard soil auger, and incorporating a few additional samples from these depths adds only modest analytical effort with rapid, portable techniques such as portable XRF and handheld LIBS, which greatly reduce the time required for bulk soil chemical characterization (Harmon, 2024; Harmon et al., 2023; Pierangeli et al., 2025). While the location of a buried dike is generally unknown during exploration, these results suggest acquiring limited profile sampling prior to large–scale composite prospecting can help identify depth–related variability and ensure that it is properly captured and interpreted. In more restrictive situations where only a single composite sample can be analyzed, it may be most effective to sample beyond the topsoil, in which surface mixing is the strongest, especially in old, residual landscapes such as the Carolina Piedmont, where hillslope processes have been prolonged and extensive.

In addition to considering Li, K/Rb, and Rb/Sr as geochemical tracers, we have demonstrated how Li isotope analysis of soils and regolith can be directly linked to pegmatite-derived signatures. Li isotopes are a powerful tool that has been applied to examine weathering dynamics across a wide range of bedrock types (Pistiner and Henderson, 2003; Huh et al., 2004; Pogge von Strandmann et al., 2019, 2020, 2021; Steinhoefel et al., 2021; Zhang et al., 2021). In our granitic pegmatite terrain, δ^7Li systematics closely reflect the contrasting weathering behaviors between above- and off-dike soils and carry the signatures of the Li-rich, weathering-resistant primary minerals, thereby providing an independent line of evidence that corroborates our geochemical and mineralogical interpretations. Although Li isotope analysis has been particularly helpful in elucidating Li behavior during soil formation, whether this can be an effective tracer for identifying Li-pegmatites in

exploration settings needs further evaluation using more comprehensive prospecting transects. Moreover, Li-isotope compositions in pegmatites and other bedrock lithologies can deviate significantly from average upper-crustal values (Teng et al., 2006), and these variations must be better constrained for soil-rock isotopic differences to be meaningfully interpreted.

Our results indicate that the interpretation that unweathered mineral particles act as a Li sink from Sirbescu et al. (2025) holds in relic landscape of the Carolina Piedmont, which has more complex pedogenic processes and more deeply weathered soils. Li-rich mineral grains from spodumene pegmatites impart Li signatures to the developing soils, making the geochemical, anomaly-based soil prospecting proposed by Harmon et al. (2025) possible in the CTSB. Although the number of independent soil profiles examined here is necessarily constrained, the observed physiochemical, mineralogical, and isotopic patterns are consistently expressed across the investigated sites and depth-resolved samples. The limited number of profiles partly reflects the logistical constraints of studying pegmatite-derived soils, for which suitable sampling locations require access to sites where drilling has independently confirmed the presence of subsurface Li-pegmatite dikes. Importantly, the pedological setting investigated here is not unique to the Southern Piedmont, as well-developed, clay-rich soils constitute nearly half of the globally documented Group 1 pegmatite deposits (Fig. 1). This global distribution suggests that deeply weathered soil-regolith systems represent an important setting for Li-pegmatite exploration and that the mechanisms observed here could extend beyond the CTSB. Therefore, testing additional paired above- and off-dike profiles across contrasting geological, climatic, and pedological settings can be an important next step for evaluating the broader applicability of this approach. In particular, tropical landscapes characterized by more advanced weathering, deeper weathering profiles, stronger bioturbation, and more extensive mixing may provide a valuable end-member for testing whether primary Li-bearing mineral signatures remain detectable in soils.

Our study provides a comprehensive pedological approach for understanding the fate of Li, one of the many critical elements essential for energy transition and emerging technologies, during weathering and soil formation. Applying similar approaches, this framework could be extended to investigate the behavior of other critical elements in weathering and soil-genesis contexts. By integrating mineralogical, textural, geochemical, and isotopic tools within a soil-regolith framework, advancing pedological and soil biogeochemical studies can better resolve how different critical metals behave in diverse landscapes and soils, building the fundamental process-level understanding to better inform future critical-metal prospecting.

5. Conclusion

Nearly half of known global Li–pegmatites are overlain by well-–developed, clay–rich soils. This study investigated the behavior of Li during soil genesis both directly above- and off-Li-pegmatite dikes under weathering conditions prevailing in the US Southern Piedmont physiographic province underlain by a basement of amphibolite and high-grade metasedimentary rock. The high solubility of Li and its weak retention on soil exchange sites lead to substantial Li losses (80.0 to 99.9 % as characterized by τ analyses) during weathering. Using physiochemical, mineralogical, size-fraction, and isotopic data, we show that the markedly high Li concentrations in above-dike soils result from Li hosted in primary minerals that have not yet been fully broken down and weathered, rather than from Li adsorbed on exchange sites, scavenged by secondary Fe, Mn, and Al oxides, or hosted in secondary clay minerals. In contrast, in off-dike soils derived from amphibolite and metasedimentary parent materials, secondary mineral phases and oxides play a more important role in retaining small to moderate amounts of residual Li. Soils reflect lithologic controls from contrasting parent materials, while pedogenic processes such as surface mixing, eluviation-illuviation, and weathering also shape the depth distribution of Li within soil profiles. Our results show strong potential for using soil Li signatures as a prospecting tool and highlight the importance of sampling depths and horizons and landscape position when interpreting soil prospecting data for a mineral exploration campaign. We encourage similar studies in other weathering and critical minerals systems.

CRediT authorship contribution statement

P. Louis Lu: Writing – review & editing, Methodology, Investigation, Formal analysis. **Russell S. Harmon:** Writing – review & editing, Methodology, Investigation, Formal analysis, Conceptualization. **Lamont Leatherman:** Writing – review & editing, Resources, Conceptualization. **Gordon D.Z. Williams:** Writing – review & editing, Methodology, Investigation, Conceptualization. **Adam C. Curry:** Writing – review & editing, Investigation, Conceptualization. **Leon Kelly:** Writing – review & editing, Investigation, Formal analysis. **Gary S. Dwyer:** Writing – review & editing, Methodology, Investigation, Formal analysis. **Valerie S. Reynolds:** Writing – review & editing, Methodology, Investigation, Formal analysis. **S. Anselme Dossou:** Writing – review & editing, Investigation. **Daniel D. Richter:** Writing – review & editing, Validation, Supervision, Resources, Project administration, Methodology, Investigation, Funding acquisition, Conceptualization.

Declaration of Generative AI and AI-assisted technologies in the writing process

During the preparation of this work, the authors used ChatGPT (OpenAI) to improve the clarity and readability of the manuscript. The authors reviewed and edited the output as needed and take full responsibility for the content of the published article.

Declaration of competing interest

The authors declare that they have no known competing financial interests or personal relationships that could have appeared to influence the work reported in this paper.

Acknowledgements

This work was supported by the NC Research Collaboratory grant on Li signatures in soils and regolith, and we sincerely appreciate and thank Piedmont Lithium Inc. for site access, sample collection, and support in kind. This work was performed in part at the Duke University Shared Materials Instrumentation Facility (SMIF), a member of the North Carolina Research Triangle Nanotechnology Network (RTNN), which is supported by the National Science Foundation (ECCS-2025064) as part of the National Nanotechnology Coordinated Infrastructure (NNCI). We thank Mr. M. Mason, Ms. E. Winter, Ms. J. M. Parker, and Mr. A. Power for their field support. We thank Mr. R. C. Hill, Dr. R. Grigoryan, Mr. C. W. Cook, Ms. Y. Hu, and Mr. R. Z. Yan for their laboratory support. We thank Dr. M.-C. Eppes and Mr. P. Webb for providing access to the petrographic microscope. We thank Drs. M. A. Kipp and C. Tu for their insightful discussions.

Appendix A. Supplementary data

Supplementary data to this article can be found online at https://doi.org/10.1016/j.geoderma.2026.118084.

Data availability

Data will be made available on request.

References

Anand, R.R., Cornelius, M., Phang, C., 2007. Use of vegetation and soil in mineral exploration in areas of transported overburden, Yilgarn Craton, Western Australia: a contribution towards understanding metal transportation processes. Geochem. Explor. Environ. Anal. 7 (3), 267–288. https://doi.org/10.1144/1467-7873/07-142.

Anderson, M.A., Bertsch, P.M., Miller, W.P., 1988. The distribution of lithium in selected soils and surface waters of the southeastern U.S.A. Appl. Geochem. 3, 205–212. https://doi.org/10.1016/0883-2927(88)90008-X.

Anderson, R.S., Anderson, S.P., Tucker, G.E., 2013. Rock damage and regolith transport by frost: an example of climate modulation of the geomorphology of the critical zone. Earth Surf. Proc. Land. 38, 299–316. https://doi.org/10.1002/esp.3330.

Ashry, M.M., 1973. Occurrence of Li, B, Cu and Zn in some Egyptian Nile sediments. Geochim. Cosmochim. Acta 37, 2449–2458. https://doi.org/10.1016/0016-7037(73)90291-3.

Černý, P., Meintzer, R. E., and Anderson, A. J. (1985). Extreme fractionation in rare-element granitic pegmatites: Selected examples of data and mechanisms. *The Canadian Mineralogist*, *23*(3), 381-421.

Černý, P., and Ercit, T. S. (2005). The classification of granitic pegmatites revisited. *Canadian Mineralogist*, *43*, 2005–2026.

Hall., G. A., Williams, G. D. Z., Sirbescu, M.-L. C., Lu, P. L., Dwyer, G. S., Richter, D. D., and Vengosh, A. (2025). Strontium isotopes and Rb/Sr Tracers in Surface soils for Locating Subsurface Lithium Pegmatites. *Appl. Geochem.*, *195*, 106631.

Bacon, A.R., Richter, D., 2012. Coupling meteoric 10Be with pedogenic losses of 9Be to improve soil residence time estimates on an ancient north American interfluve. Geology 40 (9), 847–850. https://doi.org/10.1130/G33449.1.

Banfield, J.F., Eggleton, R.A., 1988. Transmission electron microscope study of biotite weathering. Clay Clay Miner. 36, 47–60.

Beckford, H.O., Chang, C., Ji, H., 2023. Elemental behavior during weathering and pedogenesis of clay-rich red soils developed in different lithologies in Java–Madura and Sulawesi in Indonesia. Sustainability 15 (6), 4936. https://doi.org/10.3390/su15064936.

Benson, T.R., Jowitt, S.M., Simon, A.C., 2025. Special issues on the geology and origin of lithium deposits—introduction: lithium deposit types, sizes, and global distribution. Econ. Geol. 120 (3), 503–511. https://doi.org/10.5382/econgeo.5149.

Besserguenev, A.V., Fogg, A.M., Francis, R.J., Price, S.J., O'Hare, D., Isupov, V.P., Tolochko, B.P., 1997. Synthesis and structure of the gibbsite intercalation compounds [LiAl2(OH)6]X X = Cl, Br, NO3 and [LiAl2(OH)6]Cl·H2O using synchrotron X-ray and neutron powder diffraction. Chem. Mater. 9 (1), 241–247. https://doi.org/10.1021/cm960316z.

Bradley, D. C., McCauley, A. D., and Stillings, L. M. (2017). Mineral-deposit model for lithium-cesium tantalum pegmatites (Scientific Investigations Report No. 2010–5070– O), Mineral Deposit Models for Resource Assessment. US Geological Survey.

Bradley, D. C., and McCauley, A. D. (2013). A preliminary deposit model for lithium-cesium-tantalum (LCT) pegmatites. U.S. Geological Survey Open-File Report 2013–1008, 48 p.

Brady, N.C., Weil, R.R., 2017. *The nature and properties of soils*, (15th ed.). Pearson.

Brantley, S.L., Lebedeva, M., 2011. Learning to read the chemistry of regolith to understand the critical zone. Annu. Rev. Earth Planet. Sci. 39, 387–416. https://doi.org/10.1146/annurev-earth-040809-152321.

Braun, J.-J., Pagel, M., 1994. Geochemical and mineralogical behavior of REE, Th and U in the Akongo lateritic profile (SW Cameroon). Catena 21 (2–3), 173–177. https://doi.org/10.1016/0341-8162(94)90010-8.

Braun, J.-J., Pagel, M., Herbillon, A., Rosin, C., 1993. Mobilization and redistribution of REEs and thorium in a syenitic lateritic profile: a mass balance study. Geochim. Cosmochim. Acta 57 (18), 4419–4434. https://doi.org/10.1016/0016-7037(93)90492-F.

Brennan, C.J., Student, J.J., Hill, T., Martins, T., Sirbescu, M.-L.-C., 2024. Trace element concentrations and chemical zoning of spodumene from magmatic and hydrothermal origins. Ore Geol. Rev. 169, 106089. https://doi.org/10.1016/j.oregeorev.2024.106089.

Brimhall, G.H., Dietrich, W.E., 1987. Constitutive mass balance relations between chemical composition, volume, density, porosity, and strain in metasomatic hydrochemical systems: Results on weathering and pedogenesis. Geochim. Cosmochim. Acta 51 (3), 567–587. https://doi.org/10.1016/0016-7037(87)90070-6.

Buol, S.W., 2003. Formation of Soils in North Carolina. In *Papers Commemorating a Century of Soil Science*. Soil Science Society of North Carolina, pp. 31–56.

Buol, S. W., Southard, R. J., Graham, R. C., and McDaniel, P. A. (2011). *Soil genesis and classification* (6th ed.). Wiley-Blackwell. https://doi.org/10.1002/9780470960622.

Calvert, C.S., Buol, S.W., Weed, S.B., 1980. Mineralogical characteristics and transformations of a vertical rock-saprolite-soil sequence in the North Carolina piedmont: I. Profile morphology, chemical composition, and mineralogy. Soil Sci. Soc. Am. J. 44 (5), 1096–1103. https://doi.org/10.2136/sssaj1980.03615995004400050044x.

Chao, T.T., Sanzolone, R.F., 1992. Decomposition techniques. J. Geochem. Explor. 44 (1–3), 65–106. https://doi.org/10.1016/0375-6742(92)90048-D.

Curry, A.C., Wise, M.A., Harmon, R.S., 2025. Trace element geochemistry of Li-rich pegmatites in the Carolina Tin-Spodumene Belt, North Carolina, USA: implications for petrogenesis and exploration. Econ. Geol. 120 (3), 715–743. https://doi.org/10.5382/econgeo.5144.

Daniels, R.B., 1987. Soil erosion and degradation in the southern Piedmont of the USA. In: Wolman, M.G., Fournier, F.G.A. (Eds.), Land Transformation in Agriculture. John Wiley & & Sons, pp. 407–428.

Daniels, R.B., Buol, S.W., Kleiss, H.J., Ditzler, C.A., 1999. Soil systems of North Carolina (Technical Bulletin No. 314). North Carolina Agricultural Research Service. North Carolina State University.

Demetriades, A., Smith, D.B., Wang, X., 2018. General concepts of geochemical mapping at global, regional, and local scales for mineral exploration and environmental purposes. Geochim. Bras. 32 (2), 136–179. https://doi.org/10.21715/GB2358-2812.2018322136.

Deng, Y., White, G. N., and Dixon, J. B. (2023). *Soil Mineralogy Laboratory Manual*. 2023 edition. Published by the authors, Department of Soil and Crop Sciences, Texas A&M University, College Station, Texas 77843-2474.

Dietrich, W.E., Reiss, R., Hsu, M.-L., Montgomery, D.R., 1995. A process-based model for colluvial soil depth and shallow landsliding using digital elevation data. Hydrol. Process. 9, 383–400. https://doi.org/10.1002/hyp.3360090311.

Doebelin, N., Kleeberg, R., 2015. Profex: a graphical user interface for the Rietveld refinement program BGMN. J. Appl. Cryst. 48 (5), 1573–1580. https://doi.org/10.1107/S1600576715014685.

FAO, and IIASA. (2023). Harmonized World Soil Database version 2.0. Rome and Laxenburg. https://doi.org/10.4060/cc3823en.

Flesch, G.D., Anderson, A.R., Svec, H.J., 1973. A secondary isotopic standard for 6Li/7Li determinations. Int. J. Mass Spectrometry Ion Phys. 12, 265–272.

Fordham, A.W., 1990. Weathering of biotite into dioctahedral clay minerals. Clay Miner. 25 (1), 51–63. https://doi.org/10.1180/claymin.1990.025.1.06.

Gee, G.W., Or, D., 2002. Particle-size analysis. In: Dane, J.H., Topp, G.C. (Eds.), Methods of Soil Analysis: Part 4—Physical Methods. Soil Science Society of America, pp. 255–293.

Goodenough, K.M., Shaw, R.A., Borst, A.M., Nex, P.A.M., Kinnaird, J.A., van Lichtervelde, M., Essaifi, A., Koopmans, L., Deady, E.A., 2025. Lithium pegmatites in africa: a review. Econ. Geol. 120 (3), 513–539. https://doi.org/10.5382/econgeo.5133.

Grangeon, S., Bataillard, P., Coussy, S. (2020). The Nature of Manganese Oxides in Soils and Their Role as Scavengers of Trace Elements: Implication for Soil Remediation. In: van Hullebusch, E., Huguenot, D., Pechaud, Y., Simonnot, MO., Colombano, S. (eds) *Environmental Soil Remediation and Rehabilitation. Applied Environmental Science and Engineering for a Sustainable Future*. Springer, Cham.

Griffitts, W. R. (1954). Beryllium resources of the tin-spodumene belt, North Carolina: U. S. Geological Survey Circular 309, 12 p. :illus., maps (3 fold.) ;27 cm., https://doi.org/10.3133/cir309.

Harmon, R.S., 2024. Laser-induced breakdown spectroscopy in mineral exploration and ore processing. Minerals 14 (7), 731. https://doi.org/10.3390/min14070731.

Harmon, R.S., Lu, P.L., Curry, A.C., Murray, R.M., Richter, D.D., 2025. LIBS as a tool for Li-pegmatite exploration and prospect evaluation: Soil mica and soil analysis from the Carolina Tin-Spodumene Belt. Appl. Geochem. 191, 106534. https://doi.org/10.1016/j.apgeochem.2025.106534.

Harmon, R.S., Senesi, G.S., 2021. Laser-induced breakdown spectroscopy–a geochemical tool for the 21st century. Appl. Geochem. 128, 104929. https://doi.org/10.1016/j.apgeochem.2021.104929.

Harmon, R.S., Senesi, G.S., 2026. Laser-induced Breakdown Spectroscopy–*A 21st Century Analytical Tool for the Geosciences*. Cambridge Scholars Publishing, Newcastle-Upon-Tyne, UK, p. 431.

Harmon, R.S., Wise, M.A., Curry, A.C., Mistele, J.S., Mason, M.S., Grimac, Z., 2023. Rapid analysis of muscovites on a lithium pegmatite prospect by handheld LIBS. Minerals 13 (5), 697. https://doi.org/10.3390/min13050697.

Hendershot, W.H., Lalande, H., Duquette, M., 1993. Ion exchange and exchangeable cations. In: Carter, M.R. (Ed.), *Soil Sampling and Methods of Analysis*. Canadian Society of Soil Science / Lewis Publishers, pp. 167–176.

Hodges, R.A., 1983, *A petrologic study of the Lithium Corporation of America mine in the tin-spodumene belt of North Carolina*. Ph.D. thesis, North Carolina, USA, University of North Carolina at Chapel Hill, 92 p.

Horton, J.W., 1981. Shear zone between the inner Piedmont and Kings Mountain belts in the Carolinas. Geology 9 (1), 28–33. https://doi.org/10.1130/0091-7613(1981)9<28:SZBTIP>2.0.CO;2.

Horton, J. D., San Juan, C. A., and Stoeser, D. B. (2017). The state geologic map compilation (SGMC) geodatabase of the conterminous United States. U.S. Geological Survey Data Series 1052. https://doi.org/10.3133/ds1052.

Hossner, L. R. (1996). Dissolution for total elemental analysis. In D. L. Sparks, A. L. Page, P. A. Helmke, R. H. Loeppert, P. N. Soltanpour, M. A. Tabatabai, C. T. Johnston, and M. E. Sumner (Eds.), *Methods of soil analysis: Part 3. Chemical methods* (pp. 49–64). Soil Science Society of America; American Society of Agronomy. https://doi.org/10.2136/sssabookser5.3.c3.

Hoyer, M., Kummer, N.A., Merkel, B., 2015. Sorption of lithium on bentonite, kaolin and zeolite. Geosciences 5 (2), 127–140. https://doi.org/10.3390/geosciences5020127.

Huh, Y., Chan, L.-H., Chadwick, O.A., 2004. Behavior of lithium and its isotopes during weathering of hawaiian basalt. Geochem. Geophys. Geosyst. 5 (9). https://doi.org/10.1029/2004GC000729.

IEA, 2021. The role of critical minerals in clean energy transitions. International Energy Agency, Paris.

Jenne, E. A. (1968). *Controls on Mn, Fe, Co, Ni, Cu, and Zn concentrations in soils and water: The significant role of hydrous Mn and Fe oxides.* In R. F. Gould (Ed.), Trace inorganics in water (Vol. 73, pp. 337–387). American Chemical Society. https://doi.org/10.1021/ba-1968-0073.ch021.

Jochum, K.P., Nohl, U., Herwig, K., Lammel, E., Stoll, B., Hofmann, A.W., 2005. GeoReM: a new geochemical database for reference materials and isotopic standards. Geostand. Geoanal. Res. 29 (3), 333–338. https://doi.org/10.1111/j.1751-908X.2005.tb00904.x.

Jungers, M.C., Bierman, P.R., Matmon, A., Nichols, K., Larsen, J., Finkel, R., 2009. Tracing hillslope sediment production and transport with in situ and meteoric^{10} Be. J. Geophys. Res. Earth 114, F04020. https://doi.org/10.1029/2008JF001086.
Kabata-Pendias, A. (2011). *Trace elements in soils and plants* (4th ed.). CRC Press.
Kesler, T.L., 1942. *The tin-spodumene belt of the Carolinas*. U.S. Geol. Surv. Bull. 936–J, 245–266. https://doi.org/10.3133/b936J.
Kesler, T. L. (1961). *Exploration Of The Kings Mountain Pegmatites*. The American Institute of Mining, Metallurgical, and Petroleum Engineers.
Kesler, T.L., 1976. Occurrence, development, and long-range outlook of lithium pegmatite ore in the Carolinas. USGS Professional Paper 1005, 45–50.
Kim, J., Grey, C.P., 2010. ^{2}H and ^{7}Li solid-state MAS NMR study of local environments and lithium adsorption on the iron(III) oxyhydroxide, akaganeite (β-FeOOH). Chem. Mater. 22 (19), 5453–5462. https://doi.org/10.1021/cm100816h.
Kish, S. A., and Fullagar, P. D. (1996). Age and magmatic association of rare metal pegmatites; spodumene pegmatites, Kings Mountain, NC and Sn-Ta pegmatites. Rockford, AL. Geol. Soc. Am. Abstr. with Prog. 28, A475.
Kronberg, B.I., Nesbitt, H.W., Fyfe, W.S., 1987. Mobilities of alkalis, alkaline earths and halogens during weathering. Chem. Geol. 60 (1–4), 41–49. https://doi.org/10.1016/0009-2541(87)90108-2.
Li, F., Yin, H., Zhu, T., Zhuang, W., 2024. Understanding the role of manganese oxides in retaining harmful metals: insights into oxidation and adsorption mechanisms at microstructure level. Eco-Environ. Health 3 (1), 89–106. https://doi.org/10.1016/j.eehl.2024.01.002.
Li, W., Liu, X.-M., 2020. Experimental investigation of lithium isotope fractionation during kaolinite adsorption: implications for chemical weathering. Geochim. Cosmochim. Acta 284, 156–172.
Lion, L.W., Altmann, R.S., Leckie, J.O., 1982. Trace-metal adsorption characteristics of estuarine particulate matter: evaluation of contributions of iron/manganese oxide and organic surface coatings. Environ. Sci. Tech. 16 (10), 660–666. https://doi.org/10.1021/es00104a007.
London, D., 2018. Ore-forming processes within granitic pegmatites. Ore Geol. Rev. 101, 349–383. https://doi.org/10.1016/j.oregeorev.2018.04.020.
Luecke, W., 1984. Soil geochemistry above a lithium pegmatite dyke at Aclare, Southeast Ireland. Irish J. Earth Sci. 6 (2), 205–211. https://www.jstor.org/stable/30002472.
Maneta, V., Baker, D.R., 2019. The potential of lithium in alkali feldspars, quartz, and muscovite as a geochemical indicator in the exploration for lithium-rich granitic pegmatites: a case study from the spodumene-rich Moblan pegmatite, Quebec. Canada. J. Geochem. Explor. 205, 106336. https://doi.org/10.1016/j.gexplo.2019.106336.
Markewich, H.W., Litwin, R.J., Wysocki, D.A., Pavich, M.J., 2015. Synthesis on Quaternary aeolian research in the unglaciated eastern United States. Aeolian Res. 17, 139–191. https://doi.org/10.1016/j.aeolia.2015.01.011.
McBride, M.B., 1994. *Environmental chemistry of soils*. Oxford University Press.
McCracken, R.J., Daniels, R.B., Fulcher, W.E., 1989. Undisturbed soils, landscapes, and vegetation in a North Carolina Piedmont virgin forest. Soil Sci. Soc. Am. J. 53 (4), 1146–1152. https://doi.org/10.2136/sssaj1989.03615995005300040026x.
McKeague, J.A., Day, J.H., 1966. Dithionite- and oxalate-extractable Fe and Al as aids in differentiating various classes of soils. Can. J. Soil Sci. 46 (1), 13–22. https://doi.org/10.4141/cjss66-003.
Mckean, J.A., Dietrich, W.E., Finkel, R.C., Southon, J.R., Caffee, M.W., 1993. Quantification of soil production and downslope creep rates from cosmogenic ^{10}Be accumulations on a hillslope profile. Geology 21 (4), 343–346. https://doi.org/10.1130/0091-7613(1993)021<0343:QOSPAD>2.3.CO;2.
Middelburg, J.J., van der Weijden, C.H., Woittiez, J.R.W., 1988. Chemical processes affecting the mobility of major, minor, and trace elements during weathering of granitic rocks. Chem. Geol. 68 (3–4), 253–273. https://doi.org/10.1016/0009-2541(88)90025-3.
Miletić, Z., Marković, M., Jarić, S., Radulović, N., Sekulić, D., Mitrović, M., Pavlović, P., 2024. Lithium and strontium accumulation in native and invasive plants of the Sava River: implications for bioindication and phytoremediation. Ecotoxicol. Environ. Saf. 270, 115875. https://doi.org/10.1016/j.ecoenv.2023.115875.
Millot, R., Guerrot, C., Vigier, N., 2004. Accurate and high-precision measurement of lithium isotopes in two reference materials by MC-ICP-MS. Geostand. Geoanal. Res. 28, 153–159. https://doi.org/10.1111/j.1751-908X.2004.tb01052.x.
Misra, S., Froelich, P.N., 2009. Measurement of lithium isotope ratios by quadrupole ICP-MS: application to seawater and natural carbonates. J. Anal. At. Spectrom 24, 1524–1533. https://doi.org/10.1039/b907122a.
Negra, C., Ross, D.S., Lanzirotti, A., 2005. Soil manganese oxides and trace metals: competitive sorption and microfocused synchrotron x-ray fluorescence mapping. Soil Sci. Soc. Am. J. 69 (2), 353–361. https://doi.org/10.2136/sssaj2005.0353.
Noble, R.R.P., Lintern, M.J., Gray, D.G., Reid, N., Anand, R.R., 2013. Metal migration at the North Miitel Ni sulphide deposit in the southern Yilgarn Craton: Part 1, regolith and groundwater. Geochem. Explor. Environ. Anal. 13 (2), 67–85. https://doi.org/10.1144/geochem2012-132.
Noble, R.R.P., Morris, P.A., Anand, R.R., Lau, I.C., Pinchand, G.T., 2020. Application of ultrafine fraction soil extraction and analysis for mineral exploration. Geochem. Explor. Environ. Anal. 20 (1), 129–154. https://doi.org/10.1144/geochem2019-009.
O'Geen, A., Walkinshaw, M., Beaudette, D., 2017. SoilWeb: a multifaceted interface to soil survey information. Soil Sci. Soc. Am. J. 81 (4), 853–862. https://doi.org/10.2136/sssaj2016.11.0386n.
Parfitt, R.L., Childs, C.W., 1988. Estimation of forms of Fe and Al - a review, and analysis of contrasting soils by dissolution and Mossbauer methods. Aust. J. Soil Res. 26 (1), 121–144. https://doi.org/10.1071/SR9880121.
Paton, T. R., Humphreys, G. S., and Mitchell, P. B. (1995). *Soils: A New Global View (1st ed.)*. CRC Press. https://doi.org/10.1201/9781003420361.
Pierangeli, L.M.P., Sirbescu, M.-L.-C., Silva, S.H.G., Weindorf, D.C., Benson, T.R., Curi, N., 2025. Soil geochemistry toward lithium pegmatite exploration: building a machine-learning predictive algorithm via portable x-ray fluorescence. Econ. Geol. 120 (5), 1311–1330. https://doi.org/10.5382/econgeo.5166.
Pistiner, J.S., Henderson, G.M., 2003. Lithium-isotope fractionation during continental weathering processes. Earth Planet. Sci. Lett. 214, 327–339. https://doi.org/10.1016/S0012-821X(03)00348-0.
Pogge von Strandmann, P.A.E., Fraser, W.T., Hammond, S.J., Tarbuck, G., Wood, I.G., Oelkers, E.H., Murphy, M.J., 2019. Experimental determination of Li isotope behaviour during basalt weathering. Chem. Geol. 517, 34–43. https://doi.org/10.1016/j.chemgeo.2019.04.020.
Pogge von Strandmann, P.A.E., Kasemann, S.A., Wimpenny, J.B., 2020. Lithium and lithium isotopes in Earth's surface cycles. Elements 16 (4), 253–258. https://doi.org/10.2138/gselements.16.4.253.
Pogge von Strandmann, P.A.E., Renforth, P., West, A.J., Murphy, M.J., Luu, T.-H., Henderson, G.M., 2021. The lithium and magnesium isotope signature of olivine dissolution in soil experiments. Chem. Geol. 560, 120008. https://doi.org/10.1016/j.chemgeo.2020.120008.
Qi, H.P., Taylor, P.D.P., Berglund, M., De Bièvre, P., 1997. Calibrated measurements of the isotopic composition and atomic weight of the natural Li isotopic reference material IRMM-016. Int. J. Mass Spectrom. Ion Process. 171, 263–268. https://doi.org/10.1007/s002160051013.
R Core Team, 2024. *R: a language and environment for statistical computing*. R Foundation for Statistical Computing, Vienna, Austria https://www.R-project.org/.
Rebertus, R.A., Buol, S.W., 1985. Intermittency of illuviation in dystrochrepts and hapludults from the Piedmont and Blue Ridge provinces of North Carolina. Geoderma 36 (3-4), 277–291. https://doi.org/10.1016/0016-7061(85)90008-4.
Rebertus, R.A., Weed, S.B., Buol, S.W., 1986. Transformations of biotite to kaolinite during saprolite-soil weathering. Soil Sci. Soc. Am. J. 50 (3), 810–819. https://doi.org/10.2136/sssaj1986.03615995005000030049x.
Reich, M., Simon, A.C., 2025. Critical minerals. Annu. Rev. Earth Planet. Sci. 53, 141–168. https://doi.org/10.1146/annurev-earth-040523-023316.
Richter, D.D., Allen, H.L., Li, J., Markewitz, D., Raikes, J., 2006. Bioavailability of slowly cycling soil phosphorus: major restructuring of soil P fractions over four decades in an aggrading forest. Oecologia 150, 259–271. https://doi.org/10.1007/s00442-006-0510-4.
Richter, D.D., Eppes, M.-C., Austin, J.C., Bacon, A.R., Billings, S.A., Brecheisen, Z., Ferguson, T.A., Markewitz, D., Pachon, J., Schroeder, P.A., Wade, A.M., 2020. Soil production and the soil geomorphology legacy of Grove Karl Gilbert. Soil Sci. Soc. Am. J. 84 (1), 1–20. https://doi.org/10.1002/saj2.20030.
Richter, D.D., Markewitz, D., 2001. Understanding soil change: soil sustainability over millennia, centuries, and decades. Cambridge University Press.
Robinson, B.H., Yalamanchali, R., Reiser, R., Dickinson, N.M., 2018. Lithium as an emerging environmental contaminant: mobility in the soil-plant system. Chemosphere 197, 1–6. https://doi.org/10.1016/j.chemosphere.2018.01.012.
Roering, J.J., Almond, P., Tonkin, P., McKean, J., 2002. Soil transport driven by biological processes over millennial time scales. Geology 30 (12), 1115–1118. https://doi.org/10.1130/0091-7613(2002)030<1115:STDBBP>2.0.CO;2.
Roering, J.J., Kirchner, J.W., Sklar, L.S., Dietrich, W.E., 2001. Hillslope evolution by nonlinear creep and landsliding: an experimental study. Geology 29 (2), 143–146. https://doi.org/10.1130/0091-7613(2001)029<0143:HEBNCA>2.0.CO;2.
Rudnick, R.L., Tomascak, P.B., Njo, H.B., Gardner, L.R., 2004. Extreme lithium isotopic fractionation during continental weathering revealed in saprolites from South Carolina. Chem. Geol. 212 (1–2), 45–57. https://doi.org/10.1016/j.chemgeo.2004.08.008.
Rudolph, W., Brooker, M.H., Pye, C.C., 1995. Hydration of lithium ion in aqueous solution. J. Phys. Chem. 99 (11), 3793–3797. https://doi.org/10.1021/j100011a055.
Shaw, J.N., Hajek, B.F., Beck, J.M., 2010. Highly weathered mineralogy of select soils from Southeastern U.S coastal plain and piedmont landscapes. Geoderma 154, 447–456. https://doi.org/10.1016/j.geoderma.2009.01.019.
Singh, B., Gilkes, R.J., 1993. Weathering of spodumene to smectite in a lateritic environment. Clay Clay Miner. 41 (5), 624–630. https://doi.org/10.1346/CCMN.1993.0410513.
Sirbescu, M.-L.-C., Cox, T.R., Pierangeli, L.M.P., Youngblood, J.O., Weindorf, D.C., Benson, T.R., 2025. Geochemical halos in wall rocks and overlying soils as indicators of concealed lithium pegmatites. Minerals 15 (6), 615. https://doi.org/10.3390/min15060615.
Smith, D.B., Cannon, W.F., Woodruff, L.G., Solano, F., Kilburn, J.E., Fey, D.L., 2013. Geochemical and mineralogical data for soils of the conterminous United States. U.S. Geol. Survey Data Series 801, 19. https://pubs.usgs.gov/ds/801/.
Snäll, S., Liljefors, T., 2000. Leachability of major elements from minerals in strong acids. J. Geochem. Explor. 71 (1), 1–12. https://doi.org/10.1016/S0375-6742(00)00139-4.
Soil Survey Staff. (2025). Soil Survey Geographic (SSURGO) Database. United States Department of Agriculture, Natural Resources Conservation Service.
Starkey, H. C. (1982). The role of clays in fixing lithium (U.S. Geological Survey Bulletin 1278-F). U.S. Government Printing Office. https://doi.org/10.3133/b1278F.
Steinhoefel, G., Brantley, S.L., Fantle, M.S., 2021. Lithium isotopic fractionation during weathering and erosion of shale. Geochemica et Cosmochimica Acta 295, 155–177.
Swanson, S.E., 2012. Mineralogy of spodumene pegmatites and related rocks in the Tin-Spodumene Belt of North Carolina and South Carolina, USA. Can. Mineral. 50, 1589–1608. https://doi.org/10.3749/canmin.50.6.1589.
Teng, F.-Z., McDonough, W.F., Rudnick, R.L., Dalpé, C., Tomascak, P.B., Chappell, B.W., Gao, S., 2004. Lithium isotopic composition and concentration of the upper

continental crust. Geochemica et Cosmochimica Acta 68 (20), 4167–4178. https://doi.org/10.1016/j.gca.2004.03.031.

Teng, F.-Z., McDonough, W.F., Rudnick, R.L., Walker, R.J., Sirbescu, M.-L.-C., 2006. Lithium isotopic systematics of granites and pegmatites from the Black Hills South Dakota. Am. Mineral. 91 (10), 1488–1498. https://doi.org/10.2138/am.2006.2083.

Terry, R.D., Chilingar, G.V., 1955. Summary of "concerning some additional aids in studying sedimentary formations," by M S. Shvetsov. J. Sediment. Res. 25, 229–234.

Tsozué, D., Ndjigui, P.-D., 2017. Geochemical features of the weathered materials developed on gabbro in a semi-arid zone Northern Cameroon. Geosciences 7 (2), 16. https://doi.org/10.3390/geosciences7020016.

Wang, Z., Hill, R., Williams, G., Dwyer, G.S., Hu, J., Schnug, E., Bol, R., Sun, Y., Coleman, D., Liu, X.-M., Sandstrom, M.R., Vengosh, A., 2023. Lead isotopes and rare earth elements geochemistry of global phosphate rocks: Insights into depositional conditions and environmental tracing. Chem. Geol. 639, 121715. https://doi.org/10.1016/j.chemgeo.2023.121715.

Whittig, L. D., and Allardice, W. R. (1986). X-ray diffraction techniques. In A. Klute (Ed.), *Methods of soil analysis: Part 1. Physical and mineralogical methods* (2nd ed., pp. 331–362). American Society of Agronomy; Soil Science Society of America. https://doi.org/10.2136/sssabookser5.1.2ed.c12.

Wiederhold, J.G., Teutsch, N., Kraemer, S.M., Halliday, A.N., Kretzschmar, R., 2007. Iron isotope fractionation in oxic soils by mineral weathering and podsolization. Geochim. Cosmochim. Acta 71, 5821–5833. https://doi.org/10.1016/j.gca.2007.07.023.

Williams, G.D.Z., Barre, J., Louvat, P., Bérail, S., Millot, R., Vengosh, A., 2026. Geochemical controls on the formation of lithium brines in closed-basins of the Lithium Triangle. Earth Planet. Sci. Lett. 679, 119849. https://doi.org/10.1016/j.epsl.2026.119849.

Williams, G.D.Z., Saltman, S., Wang, Z., Warren, D.M., Hill, R.C., Vengosh, A., 2024. The potential water quality impacts of hard-rock lithium mining: Insights from a legacy pegmatite mine in North Carolina, USA. Sci. Total Environ. 956, 177281. https://doi.org/10.1016/j.scitotenv.2024.177281.

Wise, M.A., Harmon, R.S., Curry, A., Jennings, M., Grimac, Z., Khashchevskaya, D., 2022a. Handheld LIBS for Li exploration: an example from the Carolina Tin-Spodumene Belt, USA. Minerals 12 (1), 77. https://doi.org/10.3390/min12010077.

Wise, M.A., Müller, A., Simmons, W.B., 2022b. A proposed new mineralogical classification system for granitic pegmatites. Can. Mineral. 60, 229–248. https://doi.org/10.3749/canmin.1800006.

Xiao, M., Zhao, G., Jiang, Y., Cai, Y., Zhou, M., Cawood, P.A., Yuan, C., Cawood, I.P., Xiang, H., Zhang, W., Hong, T., 2026. Reworked staurolite-rich metamorphic belts as lithium-fertile terranes. Commun. Earth Environ. 7, 280. https://doi.org/10.1038/s43247-026-03293-6.

Xu, Z., Liang, B., Geng, Y., Liu, T., Wang, Q., 2019. Extraction of soils above concealed lithium deposits for rare metal exploration in Jiajika area: a pilot study. Appl. Geochem. 107, 142–151. https://doi.org/10.1016/j.apgeochem.2019.05.018.

Zhang, J.-W., Zhao, Z.-Q., Yan, Y.-N., Cui, L.-F., Wang, Q.-L., Meng, J.-L., Li, X.-D., Liu, C.-Q., 2021. Lithium and its isotopes behavior during incipient weathering of granite in the eastern Tibetan Plateau China. Chem. Geol. 559, 119969. https://doi.org/10.1016/j.chemgeo.2020.119969.

Zhang, X.Y., Wilson, D.J., Hamers, M.F., Pogge von Strandman, P.A.E., Mulders, J.J.P.A., Plumper, O., King, H.E., 2025. Coupling of Li–Fe: Li isotope fractionation during sorption onto Fe-oxides. ACS Earth Space Chem. 9 (1), 49–63. https://doi.org/10.1021/acsearthspacechem.4c00205.